

# **A Novel Approach to Delay Thermal and Autoxidative Fouling Caused by Aromatics in Heavy oil and Petrochemicals Using Tetrahydrofurfuryl Alcohol**

by

Ahmed Gomaa

A thesis submitted in partial fulfillment of the requirements for the degree of

**Master of Science**

**In**

**Chemical Engineering**

Department of Chemical and Materials Engineering

University of Alberta

©Ahmed Gomaa, 2023

## ABSTRACT

Tetrahydrofurfuryl alcohol (THFA) is a widely used solvent. It is a preferred solvent since it is derived from biomass. Multiple patents have reported that adding THFA during heavy oil processing improves the efficiency of the process and increases the yield. One patent for instance reported that adding THFA in a ratio of about 3wt% to feedstock decreased coke formed and increased the liquid yield of the condensable volatiles of some bitumen samples during upgrading. Another patent reported that the addition of THFA during the re-refining of oil greatly improved the efficiency of the process. The patents have yet to report anything on how THFA improves the process. Currently, there is not much literature on the use of THFA in the processing of petrochemicals. In this work, THFA was tested for its effect on the accelerated fouling of different oil samples. THFA was found to improve the autoxidative stability of the oil samples greatly reducing the amount of insolubles formed. THFA was also found to soften existing solids lightening their color and changing their physical nature to gums. THFA effect was found to be proportional to the percentage aromatics present in the oil samples. THFA was further tested on the fouling system of indene. Indene was heated with THFA at different concentration at different temperatures. It was found that THFA delayed the thermal oxidation of indene delaying the formation of carbonyl and hydroxyl groups. THFA's effect was persistent up to 230 °C. An ether compound was also tested. The ether showed similar trends to THFA; however, it was not as effective, failing to prevent oxidation at temperatures of 200 °C and above. THFA was also found to have a permanent effect on the solids formed during oxidation resulting in the formation of softer, yet denser gums than solids. THFA was found to have maximum efficiency if added in a ratio of 1:1 weight percent to the indene.

# Acknowledgments

First, I would like to thank Dr. William McCaffrey for his continuous teaching and guidance; without his knowledge and guidance, this work wouldn't have been possible.

I would also like to give special thanks to my family, which continuously supported me, especially my parents, who always encouraged me to take risks and cheered me on during the hard times of Covid.

I would like to give special thanks to my friend and colleague, Menna Ahmed, for all her help and tips on research which greatly helped me solve many problems in this project.

I would also like to thank my colleagues Sid, Daniel, Benjamin, and Gonzalo for the fun times and good chats we had in the lab.

# Table of Contents

Abstract .....	ii
Acknowledgements .....	iii
List of Tables.....	vi
List of Figures.....	vii
1 Introduction .....	1
2 Literature Review.....	3
2.1 What is Bitumen.....	3
2.2 Bitumen Upgrading .....	3
2.3 Thermal Cracking .....	4
2.4 Coke formation .....	5
2.5 Tetrahydrofurfuryl alcohol.....	12
2.5.1 Hydrogenation of Furfural .....	13
2.5.2 THFA production .....	14
2.5.3 THFA reactions .....	15
2.6 Fouling and indene.....	16
2.7 The role of additives in anti-oxidation and improving thermal stability .....	18
2.8 Characterization.....	20
2.9 Auto-oxidation in petroleum and stability.....	24
3 Experimental Procedure and Equipment.....	27
3.1 Reagents, Solvents, and gases used.....	27
3.2 Heavy Crude oil Data.....	28
3.3 Mass Scale.....	29
3.4 Micro Batch Reactor .....	29
3.4.1 Loading of the Reactor .....	30
3.4.2 Reactor Pressure .....	31
3.4.3 Heating The Reactor.....	31
3.5 Product Collection.....	33
3.5.1 Mexico Oils.....	33
3.5.2 Product collection and storing for indene. ....	34
3.6 Characterization methodology. ....	35
3.6.1 Weighing for Heavy crude oils .....	36

3.6.2	Testing Methodology for indene .....	36
3.7	Procedure and Operating Conditions. ....	37
3.7.1	Experimental Procedure .....	37
3.7.2	Table of experiments .....	38
4	Results and Discussion .....	40
4.1	Accelerated fouling of oils with THFA .....	40
4.2	Accelerated fouling of indene with THFA .....	47
4.3	Accelerated fouling of indene with THFA at higher temperatures.....	71
4.3.1	Heating indene with THFA at 200 °C.....	71
4.3.2	Heating Indene with THFA at 230 °C.....	75
4.4	Accelerated fouling of indene with ether at higher temperatures .....	78
4.4.1	Heating indene with ether at 150 °C.....	78
4.4.2	Heating indene with ether at 200 °C.....	81
4.4.3	Heating indene with ether at 230 °C.....	84
5	Conclusion.....	91

## List of Tables

Table 1: Catalyst loading vs. FA conversion and THFA selectivity for Ni- supported catalysts ....	15
Table 2: Bond frequencies which are relevant to the work. (46,47) .....	24
Table 3: Feed Stock Reagents purity, supplier, and chemical properties.....	27
Table 4: Physical and chemical properties of the heavy crude oils .....	28
Table 5: Feedstock concentrations, pressure, temperature, and residence time for indene using THFA additive.....	38
Table 6: Feedstock concentrations, pressure, temperature, and residence time for indene using Ether additive.....	39
Table 7: Feedstock concentrations, pressure, temperature, and residence time for heavy oils using THFA additive. ....	39

# List of Figures

Figure 1: Adapted Illustration of the mass transfer mechanism during coke formation from solids to liquids to the vapor phase. (adapted from (21)) .....	8
Figure 2: Coke yield vs. film thickness. (adapted from (19)) .....	9
Figure 3: Coke prevention using ethanol and a bifunctional coating. (adapted from (22)) .....	11
Figure 4: Hydrogenation of furfuryl to furfuryl alcohol and THFA. (adapted from (23)) .....	13
Figure 5: Hydrogenation of Furfuryl alcohol to THFA using Ni- Supported catalyst. ....	14
Figure 6: Oxidation mechanism of indene. (adapted from (35,54)) .....	18
Figure 7: Illustration of BMP anti-oxidation effect.(adapted from (33,54)) .....	19
Figure 8: Illustration of FTIR mechanism using carbon. (41) .....	22
Figure 9: Detailed Schematic of the micro-batch reactor. (55) .....	30
Figure 10: Schematic of the air cylinder during pressurizing the micro-reactor. (55) .....	31
Figure 11: Visual representation of the micro-batch reactor immersed in the heating sand bath .....	32
Figure 12: Visual Representation of the filter paper drying inside the oven. ....	34
Figure 13: Visual representation of collected indene products .....	35
Figure 14: Visual illustration of the paper chromatography setup .....	37
Figure 15: Insoluble collected from COND-54-NZ with and without THFA after heating .....	40
Figure 16: Insoluble collected from SLCO-43-SZ with and without THFA after heating .....	41
Figure 17: Insoluble collected from LCO-33-NZ with and without THFA after heating.....	42
Figure 18: Insoluble collected from LCO-36-MZ with and without THFA after heating.....	43
Figure 19: Insolubles collected from LCO36MZ with 10 wt% THFA without heating.....	44
Figure 20: Mass of insoluble formed with and without THFA for the oils that were heated at 150 C and at room temperature.....	45
Figure 21: Percentage aromatics by weight vs. solids prevented using THFA .....	46
Figure 22: Visual representation of indene sample after heating at 150 °C and 48 hours with no additives .....	48

Figure 23: Visual representation of aged indene sample after heating at 150 °C with no additives. The sample was aged for three months.....	49
Figure 24: Visual representation of indene sample after heating at 150 °C with 3 % THFA. The reaction time was 48 hours. ....	50
Figure 25: Visual representation of aged indene sample after heating at 150 °C with 3 % THFA. Sample aged for three months. ....	51
Figure 26: Visual representation of indene sample after heating at 150 °C with 6 % THFA. The reaction time was 48 hours. ....	52
Figure 27: Visual representation of aged indene sample after heating at 150 °C with 6 % THFA.....	53
Figure 28: Visual representation of indene sample after heating at 150 °C with 10% THFA.....	54
Figure 29: Visual representation of aged indene sample after heating at 150 °C with 10% THFA .....	55
Figure 30: Visual representation of indene solution after drying in an oven at 200 °C.....	56
Figure 31: Visual representation of 1:1 indene with THFA solution after drying in an oven at 200 °C.....	57
Figure 32: Visual representation of Chromatography paper results .....	58
Figure 33: FTIR spectra of the indene solids.....	59
Figure 34: FTIR spectra of the indene + THFA gums.....	60
Figure 35: FTIR spectra of indene solution with no additives before heating. ....	61
Figure 36: Indene FTIR spectra after heating reaction mixture at 150 °C for 48 hours. ....	61
Figure 37: aged Indene solution with no additives.....	63
Figure 38: Comparison of the indene solution before heating, after heating, and after aging ..	64
Figure 39: FTIR spectrum of the indene solution with 10% THFA before heating .....	65
Figure 40: FTIR spectrum of the indene solution with 10% THFA after heating .....	65
Figure 41: FTIR spectrum of the aged indene solution after heating with 10 wt.% THFA .....	66
Figure 42: Comparison of the indene solution with THFA before heating, after heating, and after aging.....	67
Figure 43: Indene Gum in solution (g/L) vs. time in different solvents during heating. ( adapted from (54)) .....	69

Figure 44: Autoxidation mechanism for indene(35).....	70
Figure 45: Indene plus THFA spectra after heating at 200 °C.....	71
Figure 46: Aged Indene plus THFA spectra after heating at 200 °C .....	72
Figure 47: Indene plus THFA spectra after heating at 200 °C.....	73
Figure 48 Visual representation of the aged Indene +THFA mixture after heating at 200 °C. ....	74
Figure 49: Indene +THFA spectra after heating at 230 °C.....	75
Figure 50: Aged Indene plus THFA spectra after heating at 230 °C .....	76
Figure 51: Visual representation of Indene plus THFA mixture after heating at 230 °C.....	77
Figure 52: Visual representation of the aged Indene +THFA mixture after heating at 230 °C ....	77
Figure 53: Indene + ether FTIR spectrum after heating at 150 °C for 48 hours.....	79
Figure 54: Aged indene + ether FTIR spectrum after heating at 150 °C for 48 hours.....	79
Figure 55: Visual representation of indene + ether mixture after heating at 150 °C and 48 hours .....	80
Figure 56: Visual representation of the aged indene + ether after heating at 150 °C and 48 hours .....	80
Figure 57: Indene + ether FTIR spectrum after heating at 200 °C and 48 hours.....	82
Figure 58: Aged indene + ether FTIR spectrum after heating at 200 °C and 48 hours .....	82
Figure 59: Visual representation of the indene + ether mixture after heating at 200 °C and 48 hours .....	83
Figure 60: Visual representation of the aged indene + ether mixture after heating at 200 °C and 48 hours .....	83
Figure 61: Indene plus ether FTIR spectrum after heating at 230 °C and 48 hours.....	84
Figure 62: Aged indene plus ether FTIR spectrum after heating at 230 °C and 48 hours.....	85
Figure 63: Visual representation of the indene + ether mixture after heating at 230 °C and 48 hours .....	85
Figure 64: Visual representation of the aged indene + ether mixture after heating at 230 °C and 48 hours .....	86
Figure 65: Summary of Heavy oil thermal oxidation with THFA .....	88
Figure 66: Summary of Indene thermal oxidation with THFA and Ether Additives .....	90

# 1 Introduction

Tetrahydrofurfuryl alcohol (THFA) is a widely used but relatively new solvent. It is produced from furfural, which can be produced from biomass; therefore, it is considered renewable. For this reason, THFA is gaining popularity in many chemical industries. Multiple patents have reported other benefits for THFA in a variety of applications. THFA has been reported to improve bitumen upgrading by enhancing thermal cracking by producing a higher liquid yield while reducing the amount of solid produced. THFA has also been reported to enhance the re-refining of lubricating oil by improving the product yield. THFA seems to have great industrial uses where complex organic compounds are processed. To date, there are no literature reports on how THFA improves these chemical processes or any data pinpointing a certain molecular groups that are reactive with THFA. In many cases, THFA seems to be thought of as just a solvent. Most industrial process patents report THFA as being a solvent, but no supporting chemistry is reported. Because the chemistry of how THFA affects organic molecules is unknown, the uses of THFA cannot be optimized. This thesis tests the effects of THFA on multiple organic systems to:

1. Determine organic groups on which THFA reacts.
2. Determine if THFA interacts with the system physically and if so, then how.
3. Determine if THFA interacts with the system chemically and if so, then how.

Since no literature data have been reported on the detailed chemistry of how THFA affects the systems tested, the experimental approach was initially based on trial and error. The experimental approach could be simplified into three stages

- A. Identify a possible system that is susceptible to modification with the addition of THFA and produces significant changes.
- B. Perturb the system conditions, such as temperature and pressure to be able to obtain significant products.
- C. Test the products to determine the effect of THFA on the system.

A fouling precursor, indene, was identified that is susceptible to thermo-oxidative polymerization; therefore, this thesis tests the effect of THFA on indene as a model compound (30).

Another component of this thesis is to test the effect of THFA on the autoxidation of heavy crude oils. An accelerated fouling procedure on oil samples is used to determine how effective THFA is in preventing the autoxidation of oils, to reduce fouling in pipelines and heat exchangers.

## 2 Literature Review

### 2.1 What is Bitumen

Bitumen is a type of crude oil found associated with sand deposits. Crude oil generally forms from the remains of ancient microorganisms deposited with mud and fragments of rock on the ocean bed. Over millions of years, with heat from the earth's core and pressure from the upper layers of the earth's crust, crude oils form via petrogenesis. Crude oils from around the world vary in both physical and chemical properties. Physically they range from very viscous black liquids to free-flowing straw-colored liquids. Chemically, they vary in their paraffinic, naphthenic, and aromatic content. (1)

### 2.2 Bitumen Upgrading

Bitumen extracted from oil sands has a high boiling point and contains a large fraction of complex high molecular weight hydrocarbon molecules. Depending on the extraction process used, it could contain water and solids in quantities that do not meet pipeline specifications for transportation over long distances. In general, two major options are available to prepare the oil to meet pipeline specifications, upgrading or dilution with very light oil. (2)

Upgrading of bitumen involves four steps:

1) Diluent Recovery: Where the diluent, that was used to separate the oil from the sand and then transport the bitumen to the upgrader, is removed and returned to the bitumen production facility.

2) Heavy to light Conversion; The heavy portion of the bitumen is converted into lighter hydrocarbons; two processes are generally used, thermal or catalytic cracking and fractionation. The hydrogen to carbon (H:C) ratio is improved through carbon rejection or hydrogen addition.

3) Impurity removal: sulfur, nitrogen, and metals are removed.

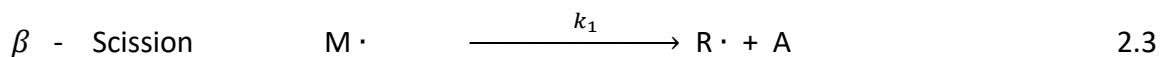
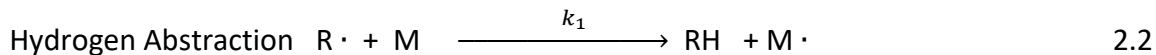
4) Product blending: The different liquid fractions produced from the upgrading process are then blended to produce desired grade of synthetic crude oil.

## 2.3 Thermal Cracking

The thermal cracking of n-alkanes occurs by a free- radical chain mechanism which was first described by Rice and Hertzfeld (3) and Kosiakoff and Rice (4). The free radical reaction mechanism can be simplified as follows. (5)



## Propagation



Where M and M · are the parent alkane radical, R · and RH are lower alkyl radicals and the corresponding alkanes, and A represents the olefins products. Alkylaromatics and saturated cyclic compounds follow similar reaction pathways (6)7). Aromatic rings exhibit resonance stabilization, hence do not thermally crack at temperatures of 410 to 550 °C. (5) At high temperatures where pyrolysis occurs, it is important to understand that a free-radical chain reaction is not the only reaction that occurs. In subsequent sections, other reaction mechanisms involving crude oil will also be discussed. (8)

## 2.4 Coke formation

Coke describes the high molecular weight carbon-rich organic matter product from thermal cracking, which is composed of poly-aromatic structures linked with aliphatic side branches. (9)

Coke has a low H:C molar ratio, so it is very carbon-rich and also contains elevated levels of heteroatoms (S, N). (10,11) Coking forms during the refining of heavy petroleum fractions and causes a variety of problems, such as fouling catalyst surfaces and blocking the active site.

(12,13) Coke also fouls the walls of process equipment.

An example of fouling due to coking happens in the catalytic hydrogenation of vacuum residue. This reaction takes place on a catalyst surface. Coke forms in the oil phase and then deposits on the catalyst surface. These deposits physically cover the active sites on the surface, inhibiting them and blocking the tiny pores on the surface. This process blocks any contact between the catalyst and the reactant, hence deactivating the catalyst. This process is called catalyst fouling.

(14-17)

The formation of coke doesn't only deactivate the catalyst but also, since the coke is part of the initial feed, directly impacts the yield of the liquid products which form during upgrading. Coke can form in the gas or the liquid phase of the mixture; however, in most applications where residence time is short, coke formation in the gas phase is minimal compared to the liquid phase. Coke yield is proportional to the molecular weight fractions and asphaltene content in the feed. (8)

A closer study of the coke formation by Goncalves *et al.* examined the asphaltene content on coke formation during the thermal cracking of different Brazilian residues. They found that the thermal cracking of Brazilian atmospheric distillation residues yielded coke which was mainly contributed by the asphaltenes content of the oil. (10, 18)

McCaffrey *et al.*, 1998 (19) observed active bubbling and evolution of products from thin films of vacuum residue under coking conditions. They observed that the coke yield depended on the thickness of the reacting films. Gray *et al.*, 2001 (20) later studied the direct relation between coking and diffusivity. They hypothesized that reducing the thickness of the reacting thin films would reduce the diffusional resistance and increase the yields of liquid. This observation suggests that coking has a dependence on the mass transfer limitations in the

system. Vafi et al. (2013) (21) summarized and explained the combination of Wiehe's theory and the hypothesis of the effect of mass transfer resistance on the yield of coke. Figure 1 shows a an adapted simple illustration of the coking mechanism from Vafi's thesis, highlighting the mass transfer resistance effect on the yield of coke. Smaller volatile products in the liquid phase move to the gas phase; during this process, they can combine using an addition reaction to form larger molecules. If they keep combining to form larger molecules, they eventually settle in a separate layer of liquid at the bottom, where the coke formation process is rapidly occurring.

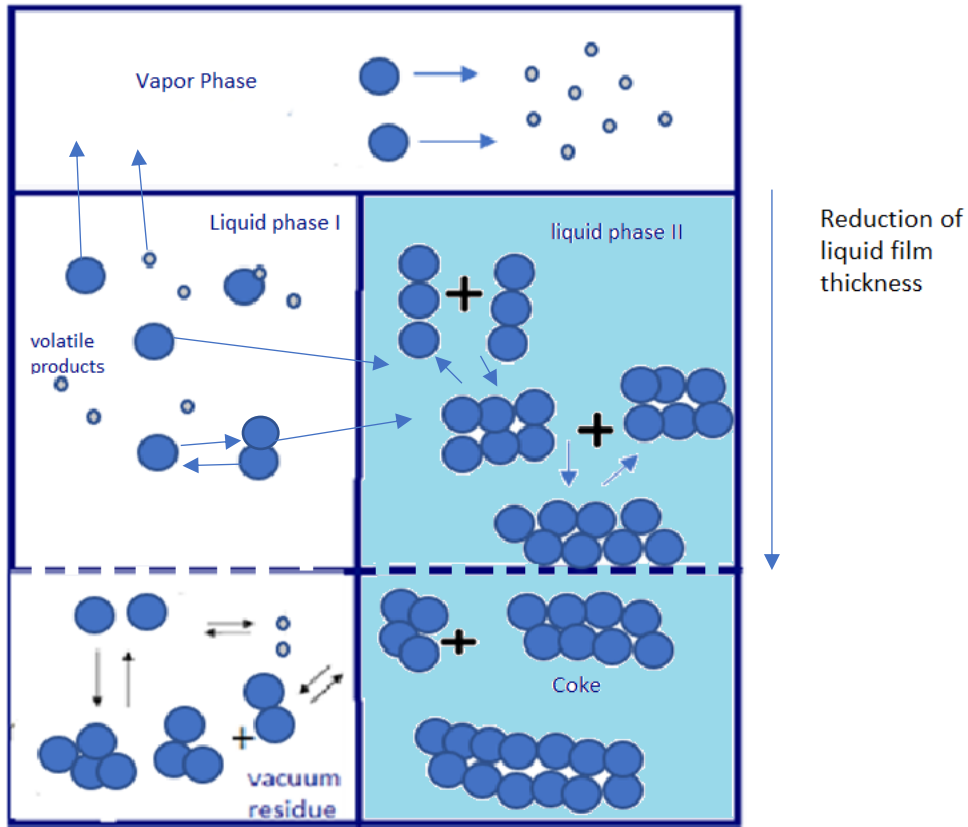


**Figure 1: Adapted Illustration of the mass transfer mechanism during coke formation from solids to liquids to the vapor phase. (adapted from (21))**

Gray et al. also succeeded in finding a relation between the liquid film thickness and coke yield.

Figure 2 shows the correlation between coke yields and film thickness.

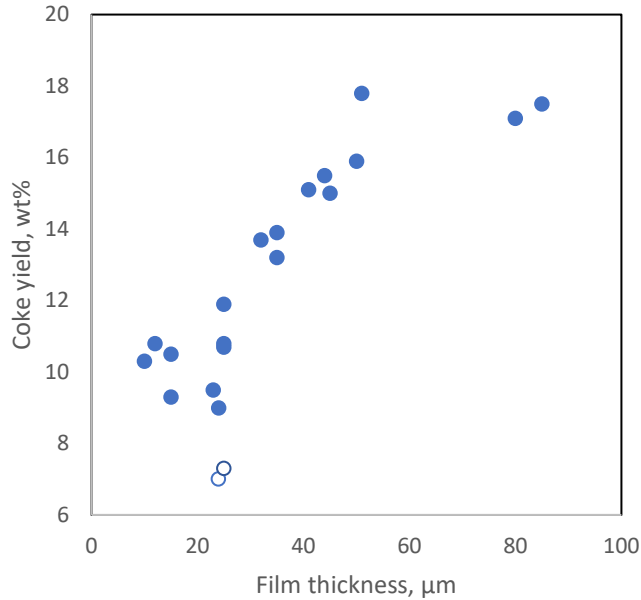


**Figure 2: Coke yield vs. film thickness. (adapted from (19))**

Gray *et al.* found that increasing the film thickness increased the yield of coke. This observation is consistent with the coupling of mass transfer and the chemical reactions leading to coke formation. During coking, the liquid phase passes through the transition from liquid to near solid as coking proceeds. This transformation increases the viscosity of the liquid layer gradually, hence reducing the diffusivity and imposing additional mass transfer resistance. This mass transfer limitation ends up trapping some of the volatile products and increases the yield of coke formation. Overall, reducing the film thickness reduces the mass transfer diffusion path imposed by the liquid phase, hence leading to less retention of volatiles or potential coke precursors in the liquid layer, and less coke yield. This observation also highlights the

importance of retrograde reactions, which could produce volatiles before coking which get trapped in the thick liquid layer and hence increases coke yield. In other words, coking is a mechanism that depends on the coupling of chemical reactions and mass transfer limitations. Both factors play a role in coke formation. Reducing coke yields could be achieved by inhibiting the chain reaction, started by coke precursors or enhancing the mass transfer of the liquid phase; this could be achieved by reducing the film thickness of the liquid phase, improving the physical properties of the liquid phase, or even completely getting rid of the liquid phase and coking at gas phase.

Since coking is a persistent problem in the petroleum industry, multiple efforts and methods have been investigated to reduce or even inhibit the production of coke. One attempt by Zhenning Yang (22) managed to achieve dramatically less coking on jet fuel cracking by using a small amount of ethanol additive over a bifunctional coating with perovskite and phosphotungstic acid. The bifunctional coating consisted of  $\text{BaWO}_4$ ,  $\text{BaCeO}_3$ ,  $\text{SiO}_2$ , and  $\text{H}_3\text{PW}_{12}\text{O}_{40}$  with an optimal ethanol amount of 5wt%. They succeeded in inhibiting coke up to 96%. Figure 3, adapted from Yang's, shows the reaction pathway of the coke-inhibiting mechanism.

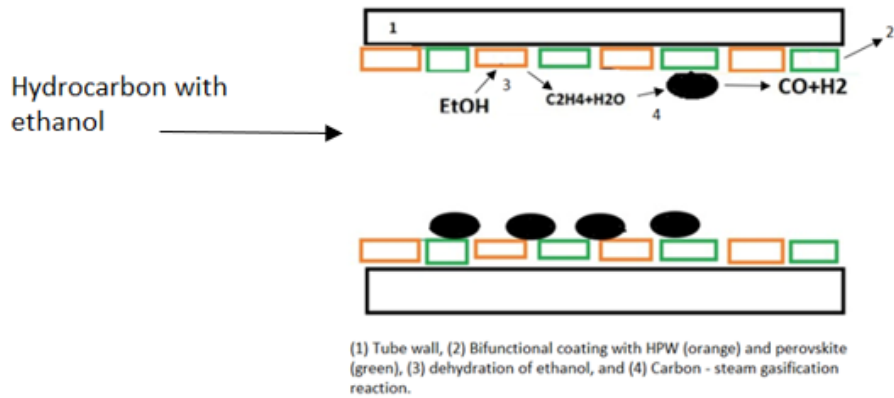


**Figure 3: Coke prevention using ethanol and a bifunctional coating. (adapted from (22))**

The importance of the bi-functional coating is that it plays an important role in insulating the active metal on the tube surface to prevent the catalytic reactions from forming filament cokes. The water generated from the dehydration of ethanol removes a considerable amount of coke deposits on the bifunctional coating.

## 2.5 Tetrahydrofurfuryl alcohol

THFA is a widely used organic solvent in many industrial applications. Since its of great importance, its syntheses by the process of catalytic hydrogenation of furfural or furfural alcohol have been industrialized. The hydrogenation of THFA from furfural happens in two steps, with furfural alcohol produced first, followed by THFA. The catalysts used are typically Pd-, Ru-, Rh-, and Ni- supported catalysts or their mixtures with Cu- supported catalysts. (23)

The hydrogenation of furfuryl alcohol in the presence of a Ni-supported catalyst has the highest yield. Nickel-on-silica-alumina catalyst containing 59% metal led to 98-99% yield and selectivity and more than 99% conversion while being able to recycle the catalytic mixture. Figure 4 shows a basic sketch of the production of THFA from raw materials through the formation of furfural or furfuryl alcohol.

## 2.5.1 Hydrogenation of Furfural

Figure 4 below shows the reaction pathway for the hydrogenation of furfural.

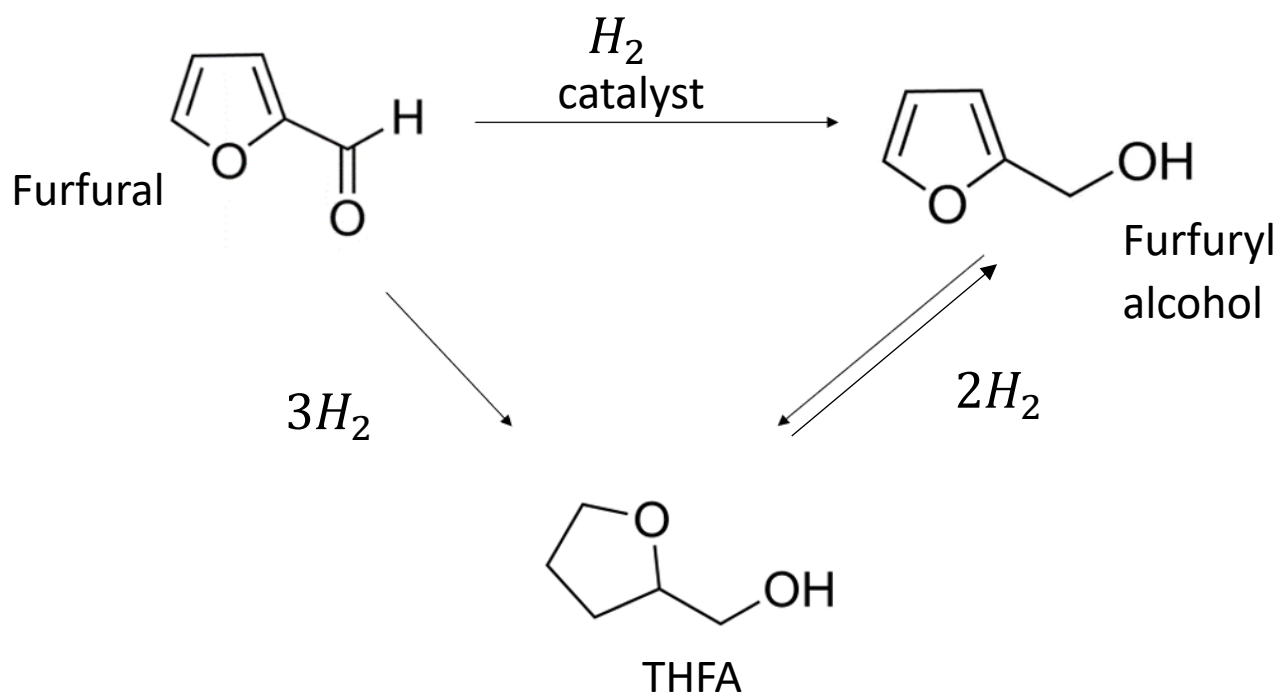


**Figure 4: Hydrogenation of furfuryl to furfuryl alcohol and THFA. (adapted from (23))**

The catalyst used in the hydrogenation of furfural to THFA is nickel-supported. Nickel could be used in the form of alloys, Raney, promoted, or supported. Nickel catalysts offered a high yield; however, the reaction was not selective. (23)

## 2.5.2 THFA production

Xiaochun (24) studied the liquid phase selective hydrogenation of furfuryl alcohol to THFA on Ni-supported catalysts. Ni supported catalysts for the conversion of furfuryl alcohol to THFA have been fully studied and industrialized. The problem with nickel-supported catalysts is that while they produce a high yield they also have low selectivity (24). Since THFA is the most preferred product of the hydrogenation of furfuryl or furfuryl alcohol, many researchers are investigating different catalysts which have promising yields as well as selectivity (24). Figure 5 shows the catalytic hydrogenation of furfuryl alcohol to THFA using a supported nickel catalyst under a pressure of 3 to 4.5 MPa and a temperature range of 430 to 460 K.

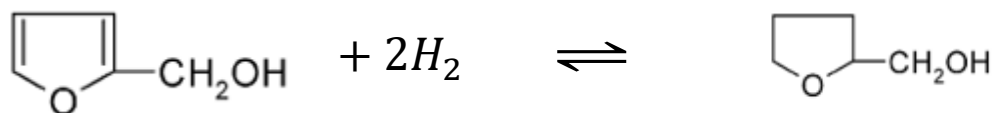


**Figure 5: Hydrogenation of Furfuryl alcohol to THFA using NI- Supported catalyst.**

Since this reaction is reversible, it gives a sense of the reactivity of THFA under these conditions, which could be useful while designing the experiment setup to understand how THFA could act under various reaction conditions.

Xiaochun studied a modified Ni-supported catalyst. They reported that the conversion of FA to THFA was highly dependent on the temperature. They also reported that catalyst loading

played a factor in the selectivity of THFA production, while the hydrogen pressure had a relatively weak impact on the hydrogenation reaction. Table 1 shows the catalyst loading effect on the FA conversion and THFA selectivity reported by Xiaochun.

**Table 1: Catalyst loading vs. FA conversion and THFA selectivity for NI- supported catalysts**

Catalyst Loading(g)	FA conversion (%)	THFA selectivity (%)
16	61.79	98.81
24	72.59	97.80
32	76.63	98.98

Another method to produce THFA is directly from furfural. (25,26) Matsagar studied the catalytic hydrogenation of furfuryl on a Rh-loaded carbon catalyst. The process was carried out under mild conditions of 30 °C in aqueous media. They reported that the catalyst showed a high yield of 92% and THFA selectivity of 93%.

### 2.5.3 THFA reactions

Wang (27) studied the hydrogenolysis of tetrahydrofurfuryl alcohol to 1,5-pentanediol over a series of carbon-supported metal/metal-oxide pairs. Wang found that Pt and Ir when paired with WO<sub>x</sub>, ReO<sub>x</sub>, and MoO<sub>x</sub> exhibited high activity and selectivity. They also found that the individual components of the catalysts exhibited low activity or selectivity, with only reducible oxides producing selective catalysts. They studied the reaction over a thin sub-monolayer of oxide on the Pt surface. Wang found that having a thin sub-monolayer of oxide over a surface of a metal is a key feature for the catalyst to exhibit activity and selectivity.

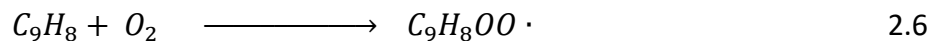
The conversion of THFA to 1,5-pentanediol was also studied by different researchers using a variety of different catalysts. Most researchers agree the use of metal oxides as catalysts produced more yield and selectivity

THFA has been reported by several patents to improve chemical processes. For instance, Delta Refining reported that the use of THFA in re-refining used lubricating oil reduced the amount of coke produced, reduced fouling on heat exchanger surfaces, improved product yield, and was recycled (28). Rival technologies also released a patent in which the use of approximately 3wt% THFA greatly improved thermal cracking. They reported that heating bitumen with THFA at 150 for 2 hours prior to cracking improved the product yield and reduced coke produced and non-distillable resins (29).

## 2.6 Fouling and indene

Autoxidation of indene has been studied by Russel. (30,31) The work reported that indene undergoes addition and abstraction reactions to form polymeric peroxides. The autoxidation of indene mainly produced polymeric indene peroxides, carbonyls, and indene hydroperoxides but not epoxides. The studies carried out by Russel were run at 50 °C. Ueno (32) analyzed the products formed by the oxidation of indene at extended times. They reported products of various carbonyls and aldehydes, which was consistent with the poly-peroxide formation and degradation. The oxidation of indene was also studied by Morris (33) and Morris and Mushrush (34), and the results were consistent with other researchers.

The auto-oxidation of indene was reported by Russel to be a bimolecular reaction of indene with oxygen to form peroxy radical.



Carlson and Robb (35) further studied the auto-oxidation of indene in excess antioxidants at 70 to 95 °C. They proposed that the auto-oxidation of indene consisted of a termolecular initiation step with two indene molecules reacting with one oxygen molecule to form indene peroxy radicals with an activation energy of 78.7 kJ/mol. They also reported that traces of hydroperoxides significantly increased the autoxidation rate. The reaction mechanism doesn't change under different initiation sources. (31) This is particularly important since this thesis discusses the auto-oxidation of indene at higher temperatures, different pressures, and with the use of an additive. Therefore, the mechanism of autoxidation could be assumed to be consistent. The mechanism was further studied by Howard and Ingold (36), who reported a ratio for addition/abstraction to be 9:1 at 30 °C. Figure 7, adapted from Wilson's thesis shows the summary of the mechanism of autoxidation of indene.

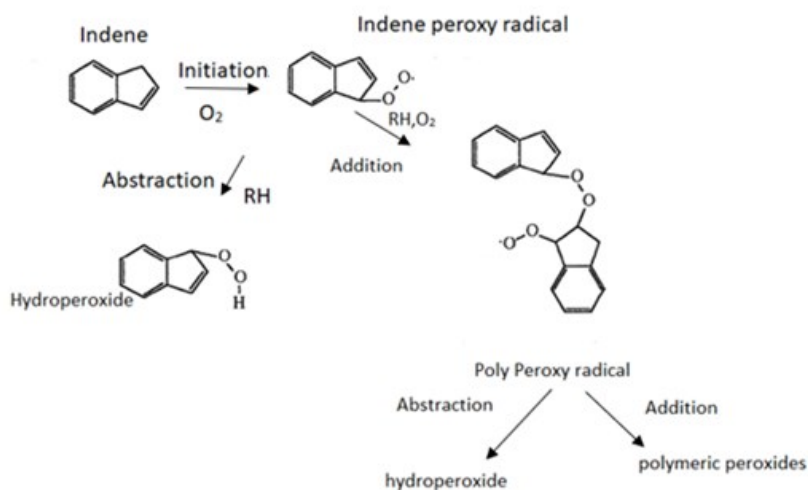


Figure 6: Oxidation mechanism of indene. (adapted from (35,54))

## 2.7 The role of additives in anti-oxidation and improving thermal stability

Additives are used to prevent the formation of permanent deposits on surfaces such as heat exchangers and hot surfaces such as reactor walls. Stephenson and Rower (37) discussed the mitigation strategies and factors that determine the choice of additives in ethene plants. They found that dispersants and detergents are used to minimize the deposition of foulant precursors. The foulant can be inhibited by the application of antioxidants or chelating agents. These compounds work by forming complexes with metal ions present in the solution. Antioxidants generally work by decomposing hydroperoxides and radical deactivation. For the hydroperoxide decomposition, the peroxides decompose to form stable products which do not form any new radicals, so the reaction is terminated. Radical scavengers can also be used that

react with the peroxy radicals to form stable species, hence achieving the same result by disrupting the chain reaction. Examples of radical scavengers (AH) are hindered phenols, amines, and some thiophenes. (38)

Below is a reaction mechanism of how radical scavengers work by forming stable products which do not further react.



Figure 8, adapted from Wilson's thesis, the reaction of the antioxidant 2,4, di-butyl-4-methyl phenol (BMP) with peroxy radicals to form stable products. (33) Antioxidants remain a very important area of research as they are temperature dependant and depend on the metal ions present in the system. For instance, BMP was only effective at temperatures below 100 °C, above which its effect was negligible.

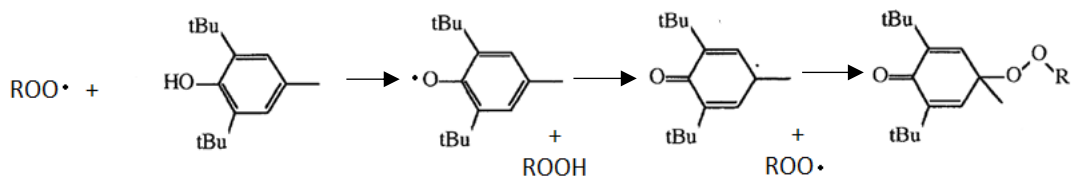


**Figure 7: Illustration of BMP anti-oxidation effect.(adapted from (33,54))**

The activity of antioxidants has been shown to be directly related to temperature. In a study by Reblova (2012), the activity of phenolic acid antioxidants was studied, which include gallic, gentisic, protocatechuic, syringic, vanillic, ferulic, caffeic, and sinapic acids. Reblova found that the activity of antioxidants decreases directly with the increase in temperature. Very low activity was detected at 150 °C, and no activity was measured beyond this temperature (39)

## 2.8 Characterization

ASTM D2274 is a standardized method for measuring the oxidative stability of heavy oils. This method incorporates aging fuel at 95 °C for 16 h while bubbling oxygen at a rate of 3L/h. The sample is then cooled to room temperature, and a vacuum filtration apparatus is used to separate the insoluble foulant products (insolubles). The insolubles are then dried, weighed, and the result is expressed as milligrams per 100mL. This number presents the total number of insolubles, which directly correlates to the oxidative stability of the oil sample at a given temperature for a given time. (40)

A powerful method to investigate the oxidative stability of oils is FTIR. Berthomieu explained the basic mechanism of how FTIR works using a carbon atom as a model (41). Infrared spectroscopy probes the molecular vibrations to determine functional groups. Each functional group is characterized by a unique infrared absorption band, which corresponds to the vibrations of the functional group. (42,43) The vibrations could be classified as infrared active or

infrared inactive. An infrared inactive corresponds to a bond where there is no change in the dipole moment between the two molecules forming the functional group such as a symmetric vibration. For example, two similar molecules form a bond, as in oxygen or nitrogen. An infrared-active molecule is a normal mode of vibration; this is created when there is a change in the dipole moment of the molecule during the vibration. Infrared inactive bonds are not detected by FTIR spectroscopy. In simpler terms, if a molecule has a center of symmetry, all vibrations which are symmetrical with respect to the center are infrared inactive; in contrast, all asymmetric vibrations of all molecules are infrared active. Groups with permanent dipoles like polar bonds exhibit very strong IR absorptions. In the mid-infrared wavelength region, there are two types of vibrations. Vibrations along chemical bonds are referred to as stretching vibrations. These vibrations involve bond-length changes. The second type of vibrations are vibrations involving changes in bond angles.

The stretching vibrations could be modeled using the basic harmonic oscillator model. In this model, the chemical bond between two molecules is represented by two-point masses linked by a spring. The bond strength is represented by the tenseness constant  $k$ . The two masses ( $m_1$  and  $m_2$ ) model the masses of the two molecules or the chemical groups

The vibration frequency could be measured using the following equation. (41)

$$v = \left( \frac{1}{2\pi c} \right) \sqrt{\left( \frac{k(m_1 + m_2)}{m_1 m_2} \right)} \quad 2.9$$

The vibrational frequency  $\nu$  depends on the bond strength. This means that triple bonds will have a higher frequency than double bonds and single bonds, respectively. Figure 9 below illustrates the concept of vibrational frequency for a CO bond.

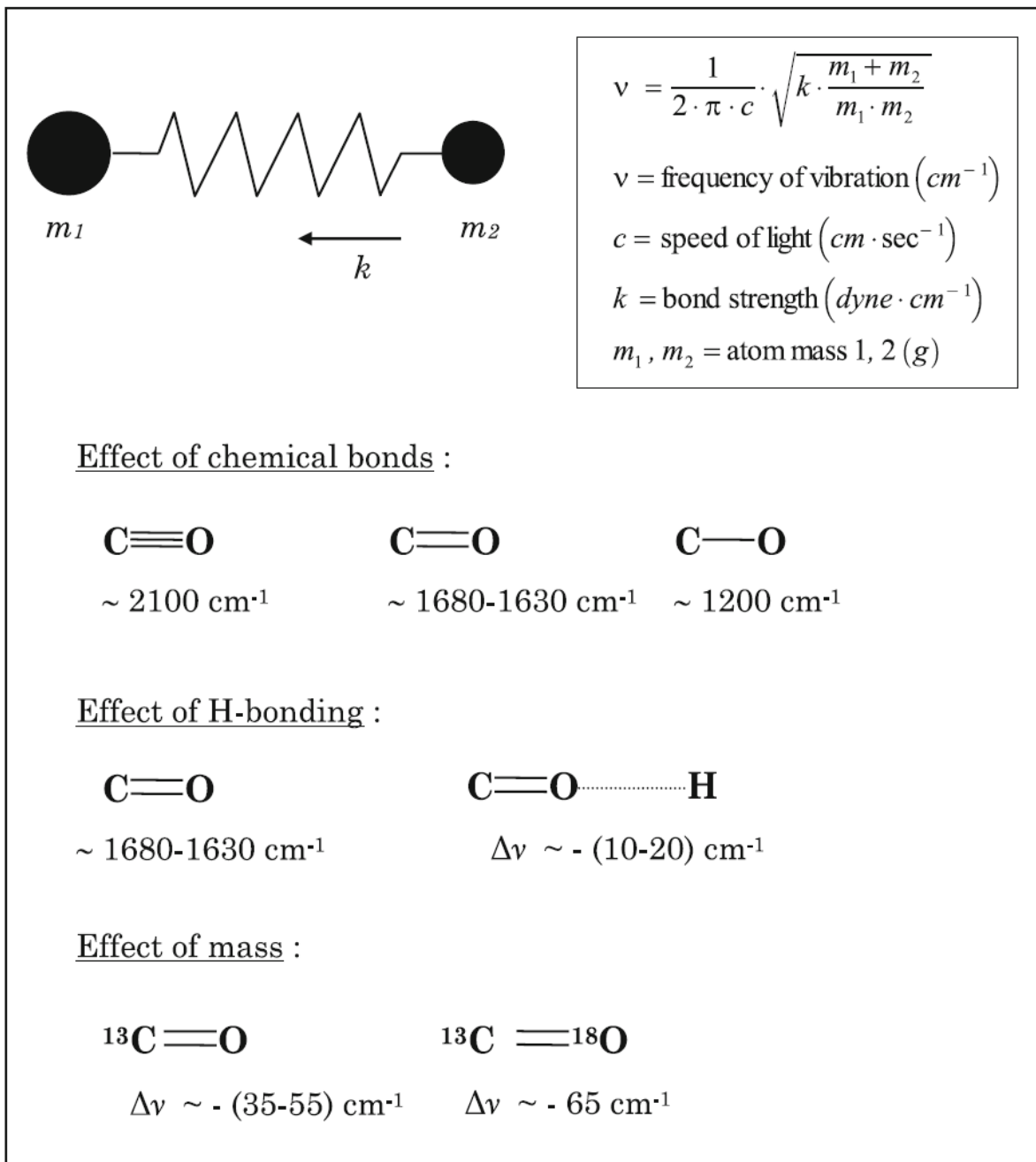


Figure 8: Illustration of FTIR mechanism using carbon. (41)

Since the frequency of the stretching depends on the bond strength, this means that the frequencies are very sensitive to the group environment; in other words, the bonds around the functional group, as illustrated in Figure 9, H bonding changed the frequency of the double bond between the carbon and the oxygen atom. The presence of the H – bonding induced a weakening of the bond strength of the carbon-oxygen double bond; this means the vibrational frequency changed or, in other words, was downshifted. This is very practical since FTIR is done before and after a procedure and could indicate whether new bonds are forming from clues like new peaks developing or existing peaks shifting. The sensitivity of the FTIR method is high and responds to changes in bond length smaller than 0.2 Å. (44,45)

As Illustrated by Figure 9, the mass of the atoms forming the bond makes a difference in the vibrational frequency; for instance, a carbon -13- isotope exhibited a different frequency than that of a carbon-12 atom. The most common functional groups have been well studied, and tables have been published with the most vibrational frequency of these functional groups. (41) Table 2 shows different Bond lengths' vibrational frequencies for functional groups relevant in this study.

**Table 2: Bond frequencies which are relevant to the work. (46,47)**

<b>Absorption (cm<sup>-1</sup>)</b>	<b>Group</b>	<b>Compound Class</b>
<b>3550-3200</b>	O-H	alcohol
<b>3060-3040</b>	C-H	aromatic
<b>1815-1650</b>	C=O	aromatic

## 2.9 Auto-oxidation in petroleum and stability

The autoxidation of petroleum fuels is a longstanding problem that occurs during oil storage.

This issue is characterized by a slow self-oxidation mechanism. The underlying mechanism has not been thoroughly investigated and may occur in an otherwise seemingly stable environment.

Autoxidation alters the chemical structure of the stored fuel and, in turn, changes its reactivity and potential uses, which affect its product qualities.

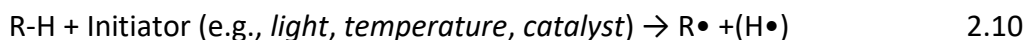
Since the mechanism is not very well known, it is difficult to predict the duration of the storage for certain fuels or to control the aging of fuels. The autoxidation process depends on the components of the fuel, for example, the presence of compounds containing heteroatoms of oxygen, sulfur, nitrogen, or traces of metals could potentially catalyze the aging. Physical storage conditions such as light exposure, temperature, and oxygen source also play a vital role in the aging of fuels. (48)

The presence of hydrocarbons in the fuel, which are the essential components of petroleum-based fuels, accelerates the aging process. The hydrocarbons react with oxygen found in the air

and with each other, producing different products in the fuel. Oxygenation products undergo further changes resulting in a change of coloration, production of gums, and formation of sediments and solids. (49)

There are many theories about the oxidation mechanism of hydrocarbons; one theory is explained by Backstrom (50), which is based on the chain mechanism radicals that form due to initiators such as light, temperature, or catalysts. The proposed chain reaction is explained below.

**a. Initiation:**



**b. Propagation:**



**c. Termination:**



**d. Chain branching:**



wherein: R-H – denotes hydrocarbon,

R• – hydrocarbon radical, R-O-O• – peroxide radical, R-O-O-H – hydroperoxide.

The reaction starts with an initiation step generating hydrocarbon free radicals. This step is very slow and is usually initiated at ambient temperatures. The rate of this step could also be increased by an increase in temperature or the presence of metal traces that catalyzes the free radical generation. The chain growth step follows the initiation step. In this step, two reactions occur, with the first reaction consisting of the free radical reacting with molecular oxygen present forming a peroxide radical, and the second reaction is the rate-determining reaction of the chain growth step, and it consists of the peroxide radical attaching to a hydrogen atom after detaching it from another hydrocarbon molecule. This step results in the production of a peroxide and a free radical hydrocarbon which repeats the procedure of the initial free radical. The termination step consists of recombination between the radicals and the decomposition of the hydroperoxides to form non-radical products such as alcohols, ketones, or acids.

For auto-oxidation to take place, conditions that enable the formation of free radicals need to exist for the process to be initiated. These conditions include but are not limited to the pressure of oxygen, the temperature range, the presence of hydroxides, active metal ions, water, microorganisms, or light (51). At temperatures higher than 150 °C, cleavage of the O-O bond could occur, which further reduces the stability of the fuel.

Two types of gasoline with octane numbers (RON) of 95 and 98 were tested for their autoxidation chemistry for a period of 6 months. (52-54) FTIR spectral analysis indicated an increase in the OH peak at 3330  $\text{cm}^{-1}$  as storage time increases. The samples in the published

study had added ethanol; however, the increasing intensity trend in the OH peak suggested that oxidation led to the formation of hydroxyl groups. The formation of gums was also observed over the aging process. FTIR spectral analysis also indicated that the area under the  $1743\text{ cm}^{-1}$  peak increased, likely due to the formation of carbonyl groups. (48)

### 3 Experimental Procedure and Equipment

#### 3.1 Reagents, Solvents, and gases used.

Mexican crude oils and indene were used as reactants. THFA was used as an additive, and kerosene was used as a solvent medium in all experiments which did not involve Mexican crude oils. Table 3 shows all the liquid and gas reagents used and their purities.

**Table 3: Feed Stock Reagents purity, supplier, and chemical properties**

Reagent	Role	Supplier	Boiling point(°C)	purity
<b>Indene</b>	Reactant	TCI America	181	>93%
<b>THFA</b>	Additive	TCI America	178	>98%
<b>Kerosene</b>	Solvent medium	WOODS	variable	NA
<b>Air (Compressed)</b>	Oxygen source		NA	
<b>1,4-Butanediol</b>	Additive	Thermo	235	>96%
<b>monomethyl Ether</b>		Scientific		

## 3.2 Heavy Crude oil Data

Table 4 shows all the physical properties as well as a brief chemical and physical composition of the heavy crude oils used in this study.

**Table 4: Physical and chemical properties of the heavy crude oils**

Oil	COND54NZ	LCO33NZ	LCO36MZ	SLCO43NZ
<b>Spec Gravity API</b>	49.0	31.3	37.1	42.5
<b>Specific gravity @ 20/4 °C</b>	0.7805	0.8661	0.8364	0.81
<b>15.6°C</b>				
<b>21.1°C</b>				
<b>25.0 °C</b>	1.983	15.43	5.096	13.85
<b>37.8°C</b>	1.593	9.674	3.615	8.934
<b>54.4°C</b>	1.248	6.215	2.764	5.844
<b>70.0°C</b>				
<b>Nickel, ppm</b>	0.3	9.8		11.0
<b>Vanadium, ppm</b>	1.6	73.7		55.9
<b>Paraffin content</b>	1.92	3.895	2.56	1.704
<b>Insoluble in C7, % weight</b>	0.19	1.87	0.4	2.03
<b>Salt content, Lb / 1000 bls</b>	12.98	26.1	2.767	25.73
<b>Distillation water, % vol.</b>	0.13	0.1	0.05	0.05
<b>Sediments by extraction, % mass.</b>	0.004	0.017	0.005	0.006
<b>Total nitrogen, ppm</b>	88	1425	541	1528
<b>Total sulfur, wt%</b>	0.198	2.299	0.981	1.966
<b>C, wt%</b>	85.69	85.08	86.58	86.25
<b>H, % weight</b>	14.1	12.41	12.36	11.56
<b>Insoluble in n-C5, % weight</b>	1	13.3	1.62	6.12
<b>Saturated, % weight</b>	69.67	36.08	50.56	40.28
<b>Polar, % weight</b>	6.11	20.17	11.74	20.14
<b>Aromatics, % weight</b>	22.94	30.45	36.08	33.46
<b>Intrinsic stability, S (ROFA)</b>	6.0	3.1	2.0	2.4

### 3.3 Mass Scale

METLER AL204 mass scale with an uncertainty of 0.001 g was used to weigh the reactants and products. Both the reactants and the additive were transferred to a glass vial using a pipette until the desired weight was reached. The vial is then sealed and shaken until all the liquid reagents are evenly mixed. The contents of the vial are then poured into the micro-batch reactor. The figure below shows the weighting procedure.

### 3.4 Micro Batch Reactor

Figure 10 shows a detailed schematic of the batch microreactor used. The micro-reactors were used for all high-temperature reactions where the temperature was equal to or exceeded 100 °C. The pressure inside the microreactor was kept constant for all experiments at 750 Kpa cold air pressure.

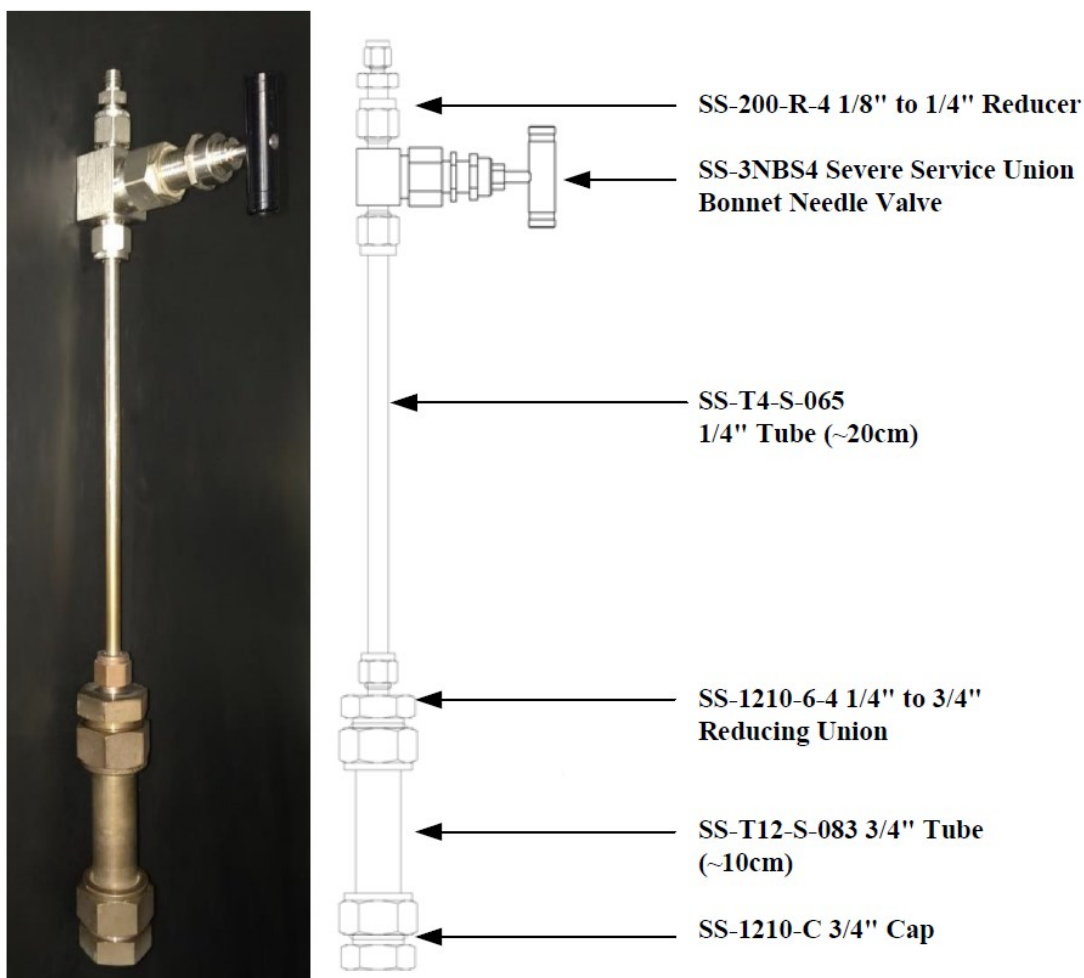


**Figure 9: Detailed Schematic of the micro-batch reactor. (55)**

### 3.4.1 Loading of the Reactor

The liquid reagents were loaded into the microreactor using a combination of a pipette and a small flask. The contents were transferred from the vendor bottles to the flask using a pipette, the flask was then placed inside a scale, and the mass was adjusted using the pipette by removing excess or adding extra until the desired weight was reached. Once the desired weight is reached, the contents of the flask are shaken to allow proper mixing, then transferred to the microreactor inside the fume hood. The microreactor is then sealed and placed inside the

preheated sand bath. Below is a diagram illustrating the flask while it is being weighted using the scale placed inside the fume hood.

### 3.4.2 Reactor Pressure

After the reactor is sealed, it is pressurized using air from the high-pressure cylinders, as illustrated in figure 11.

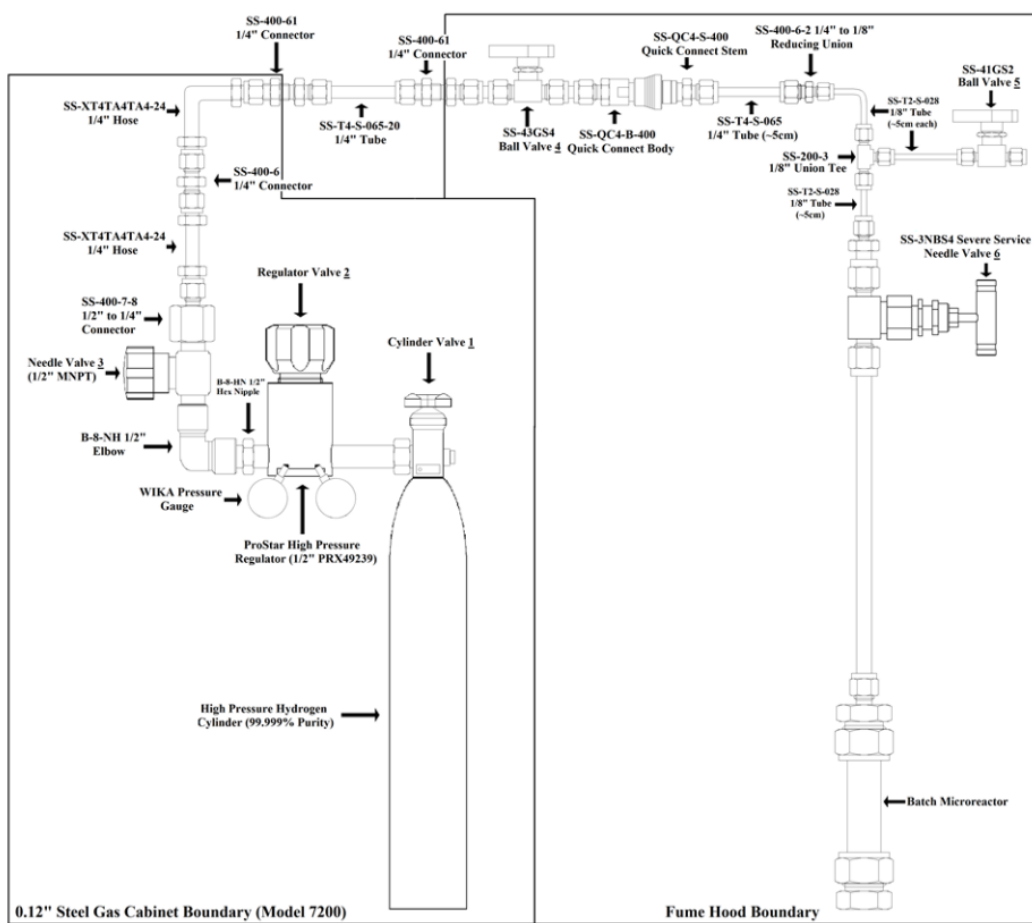


Figure 10: Schematic of the air cylinder during pressurizing the micro-reactor. (55)

### 3.4.3 Heating The Reactor

Figure 12 shows the Cole Parmer Techne fluidized sand bath that was used to heat the micro-reactors. No mixing was needed due to all the reagents being homogenous; hence the agitator

attached was not turned on, and the reactor was still in the fluidized bed. The bath was filled with approximately 25 cm of 96%  $\text{Al}_2\text{O}_3$  from the bottom; this was enough to immerse the entire length of the micro-batch reactor. The bed was fluidized using air at a flow rate of 40 LPM. The temperature was controlled using a thermocouple immersed in the sand attached to an OMRON E5CK temperature controller. Figure 12 below shows the reactor immersed in the sand bath.



**Figure 11: Visual representation of the micro-batch reactor immersed in the heating sand bath**

## 3.5 Product Collection

### 3.5.1 Mexico Oils

#### 3.5.1.1 Vacuum Filtration apparatus

A vacuum filtration setup was used to filter the oil products. An EMERSON nonreversible motor was used, model S55MTN-6867, with a 0.25 HP, 115 V, and 5A. 0.45  $\mu\text{m}$  HVLP filter paper was used to collect solids.

#### 3.5.1.2 Drying of filter paper

The drying of the filter paper was carried out in a sealed oven. The temperature of the oven was very crucial to this experiment. The filter paper was still wet after filtration, with a large surface area; if the temperature of the oven is higher than the reactor temperature, further oxidation could take place since the filter paper is in contact with air; if the temperature of the oven is very low, time for drying would be long, hence, another possibility for a reaction. While further oxidation would not necessarily change the weight of the solids collected, it could, for instance, change the visual observation of the physical characteristics of the product. A temperature of 100 °C and 15 mins were sufficient to dry the filter paper without any further physical change to the appearance of the gums. Figure 13 below shows the drying of the filter paper in the oven and visualizes how much air is in contact with the filter paper.



**Figure 12: Visual Representation of the filter paper drying inside the oven.**

### 3.5.2 Product collection and storing for indene.

Since the indene solution was observed visually, the products from the reactor were carefully transferred to a transparent glass vial, as shown in Figure 14. The contents of the vial were visually monitored inside a fume hood for further evaluation.



**Figure 13: Visual representation of collected indene products**

### 3.6 Characterization methodology.

The testing and characterization methodology was done differently for indene and for the Mexican oils. In indene, the samples were monitored visually since the system takes much longer to yield solids and even longer when THFA is added. It was very hard to determine exactly when the auto-oxidation reaction had stopped, so for indene; the system was observed

visually comparing the vials which contained THFA vs. those that did not contain THFA. As for Mexican oils, the system would yield solids much faster, so it was a better method to immediately weigh the solids formed

### 3.6.1 Weighing for Heavy crude oils

For the heavy oils, the product is very sticky; hence it is transferred immediately to the vacuum filtration apparatus and monitored until completely filtered. After drying the filter papers in the oven, the weight is recorded.

**Weight of residue = weight of filter paper before filtering – the weight of filter paper after drying**

### 3.6.2 Testing Methodology for indene

Qualitative chemical and physical tests were performed on the indene product.

#### 3.6.2.1 Thin-layer Paper chromatography

Silica gel 60 F<sub>254</sub> TLC paper was used. The solvent used was 40% Toluene, 40% Heptane, and 20% 2-propanol. Figure 15 shows the TL paper chromatography apparatus.

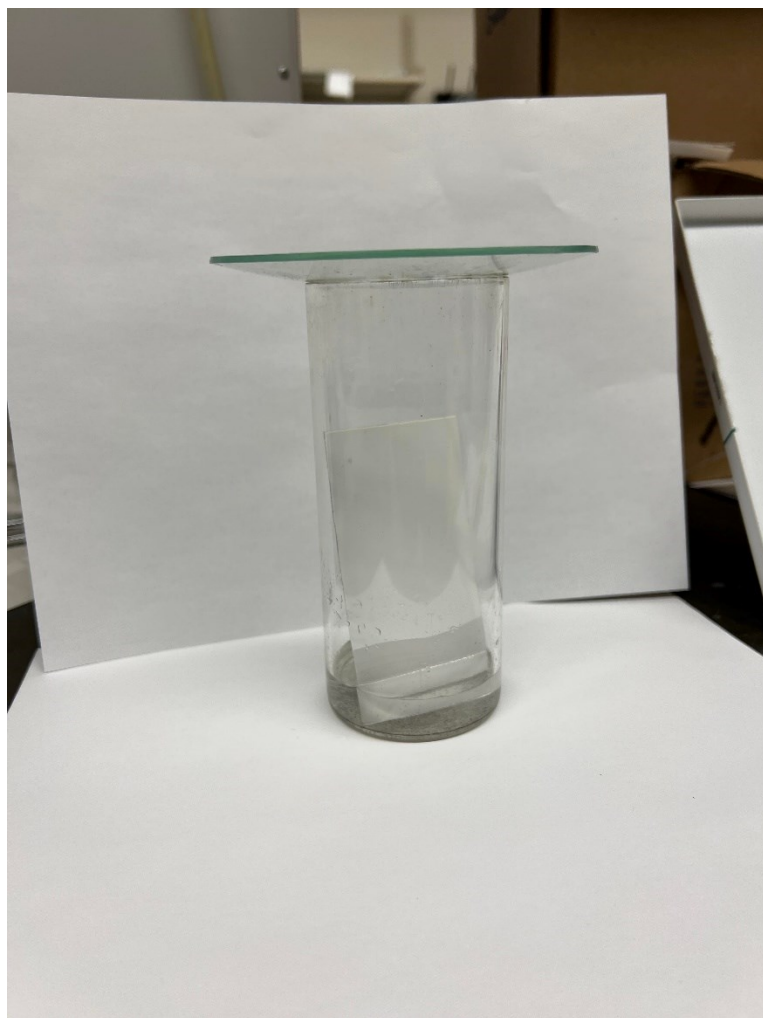


**Figure 14: Visual illustration of the paper chromatography setup**

### 3.6.2.2 FTIR

An ALPHA FTIR base spectrometer with a ZnSe optics system was used. A non-destructive method for liquids only was used to detect all the functional groups present in the liquid phase.

## 3.7 Procedure and Operating Conditions.

### 3.7.1 Experimental Procedure

The reaction procedure was very simple, consisting of 3 stages. The first step was preparing the feedstock. This was done using a pipette to carefully add the reagents to glass vials inside the

mass scale. The vials were then shaken and transferred to the micro-batch reactor; the process was very safe and simple and was carried out using vinyl gloves.

The second step was sealing the reactor, then pressurizing it using the air pressure system explained earlier in Figure 11. The reactor is then placed in the heated sand bath. The temperature of the sand bath varied depending on the desired conditions. Tables 3.3 to 3.5 show a summary of the feedstock, pressure, temperature, and residence time inside the micro-batch reactors.

The final step was quenching the reaction; this was done by removing the reactor from the sand bath and placing it in front of a cold air hose until it was brought to room temperature.

The contents of the reactor were then emptied, and the appropriate characterization methods described earlier were applied.

### 3.7.2 Table of experiments

Tables 5,6, and 7 show a summary of the experiments with their respective reagent concentrations and reaction conditions.

**Table 5: Feedstock concentrations, pressure, temperature, and residence time for indene using THFA additive.**

Experiment	Weight % of indene	Weight % of THFA	Weight % of solvent	Pressure, cold (Kpa)	Temperature (°C)	Reaction time (Hrs.)	Total weight of solution (grams)
1	10	3	87	750	150	48	10
2	10	6	84	750	150	48	10
3	10	10	80	750	150	48	10
4	10	0	90	750	150	48	10
5	10	10	80	750	150	48	10
6	10	10	80	750	200	48	10
7	10	10	80	750	230	48	10

**Table 6: Feedstock concentrations, pressure, temperature, and residence time for indene using Ether additive.**

Experiment	Weight % of indene	Weight % of ETHER	Weight % of solvent	Pressure, cold (Kpa)	Temperature (°C)	Reaction time (Hrs.)	Total weight of solution (grams)
8	10	10	80	750	150	48	10
9	10	10	80	750	200	48	10
10	10	10	80	750	230	48	10

**Table 7: Feedstock concentrations, pressure, temperature, and residence time for heavy oils using THFA additive.**

Experiment	Oil	Weight of THFA (g)	Weight of oil (g)	Pressure, cold (kPa)	Temperature (°C)	Reaction time (Hrs.)
11	COND54NZ	1	9	750	150	2
12	COND54NZ	0	10	750	150	2
13	LCO33NZ	1	9	750	150	2
14	LCO33NZ	0	10	750	150	
15	LCO 36 MZ	1	9	750	150	2
16	LCO36MZ	0	10	750	150	2
17	SLCO43MZ	1	9	750	150	2
18	SLCO43MZ	0	10	750	150	2
19	LCO36MZ	1	9	No Pressure	25	2
20	LCO36MZ	0	10	No Pressure	25	2

## 4 Results and Discussion

### 4.1 Accelerated fouling of oils with THFA

Since THFA was reported to improve the efficiency of upgrading, increasing liquid yield, and improving the efficiency of refining, an accelerated fouling system was designed and built to observe the effect of THFA on the oils firsthand. Different oil samples with varying densities and aromatic contents were tested using the accelerated fouling method. The oils were heated at 150 °C for 2 hours at 750 kPa cold air pressure with and without THFA. The figures below show the visual representation of the insoluble collected from the thermally oxidized oils. Figures 16, 17, 18, and 19 show two filter papers where the solids were collected from heating with and without THFA.



**Figure 15: Insoluble collected from COND-54-NZ with and without THFA after heating**

The addition of THFA to the crude oil sample had a remarkable impact on the visual appearance of the products, as can be seen in Figure 16. Heating with THFA yielded 0.0264 g of solids, while heating without THFA yielded 0.0342 g of solids. Heating with THFA also yielded a filter paper with a very faded yellow-brown color, while heating without THFA yielded a very dark brown-black filter paper.



**Figure 16: Insoluble collected from SLCO-43-SZ with and without THFA after heating**

Heating with THFA yielded 0.0613 grams of solids, while heating without THFA yielded 0.1867 grams of solids. Similar to the results from the COND-54-NZ crude oil, heating with THFA also yielded a filter paper with a very faded yellow-brown color, while heating without THFA yielded a very dark brown-black filter paper. Remarkably, both filter papers show a striped pattern. This pattern was only observed with THFA and not seen previously in our laboratory. The factors that caused the pattern were not determined as part of this thesis.

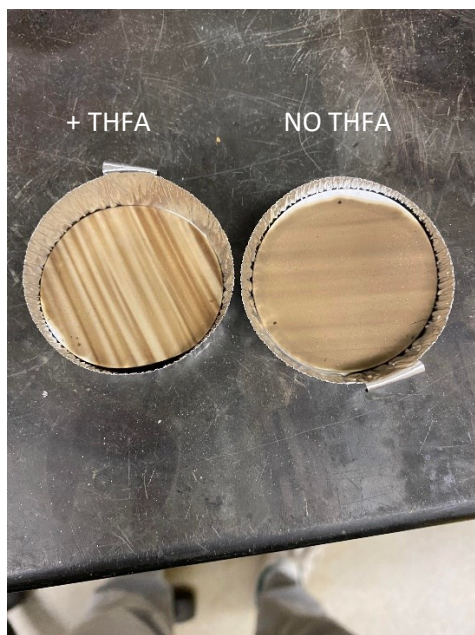


**Figure 17: Insoluble collected from LCO-33-NZ with and without THFA after heating**

Heating with THFA yielded 0.0206 grams of solids, while heating without THFA yielded 0.0855 grams of solids.



**Figure 18: Insoluble collected from LCO-36-MZ with and without THFA after heating**

Heating with THFA yielded 0.0616 grams of solids, while heating without THFA yielded 0.1416 grams of solids. Heating with THFA also yielded a filter paper with a very faded yellow-brown color, while heating without THFA yielded a very dark brown-black filter paper.

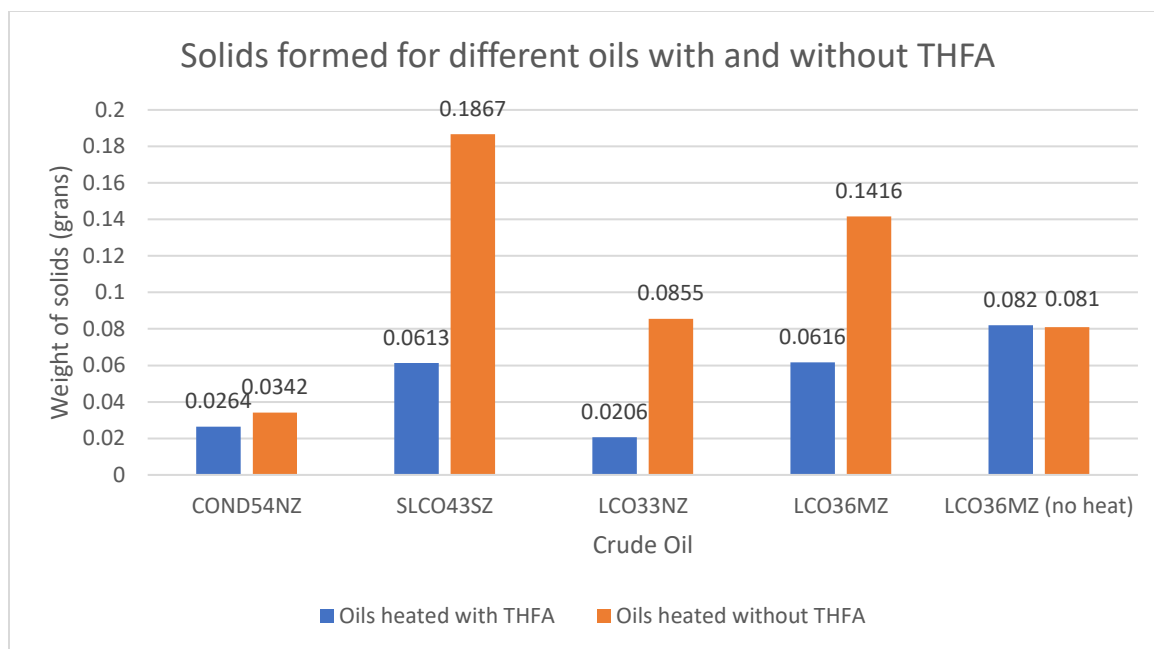
The presence of THFA during heating greatly reduced the mass of solids on the filter paper on all four oils tested, as well as changing the nature of solids from dark solids to lighter color gums. Figure 20 below shows a control experiment done on LCO36MZ without heat



**Figure 19: Insolubles collected from LCO36MZ with 10 wt% THFA without heating**

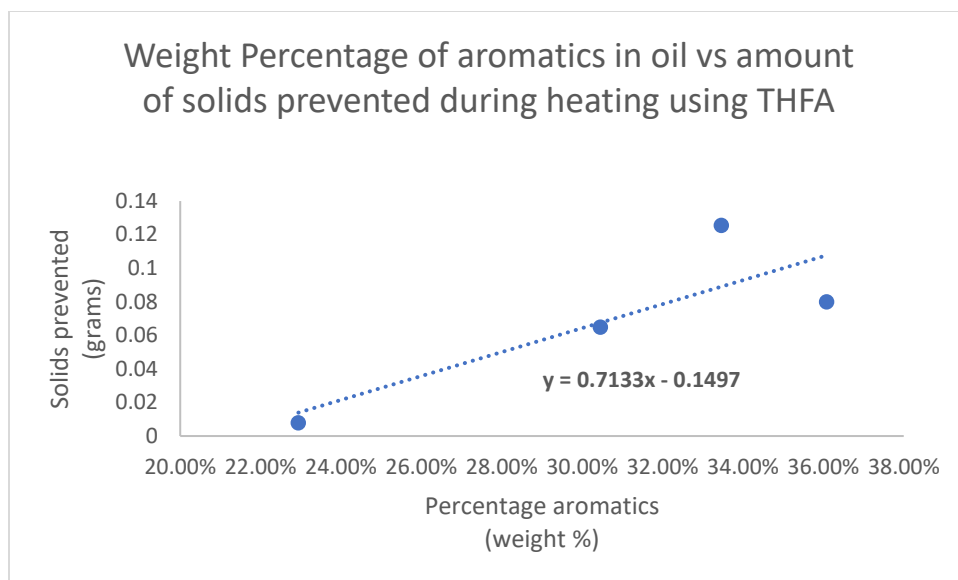
A control experiment was conducted with LCO36MZ with no heat. This experiment yielded very interesting results regarding the effect of THFA. The filter paper on the left in Figure 20 is the filter paper after drying with no THFA and on the right with THFA. Using THFA, the product weight was 0.082 g, and without THFA, the product weight of 0.081 g. At the lower temperature, THFA did not change the amount of insoluble produced; however, a very important observation here is that the filter paper where THFA was used has a much lighter color to it. While THFA did not reduce the quantity of filterable solids in the system, it did change the morphology of the solid from a solid to a gum.

Figure 21 shows a comparison of the amount of insoluble collected with and without heat for all the samples.



**Figure 20: Mass of insoluble formed with and without THFA for the oils that were heated at 150 C and at room temperature.**

Figure 22 shows the weight percent aromatic component of the oil vs. the weight of insoluble prevented during heating. From Figure 22, it can be deduced that the effect of THFA is proportional to the number of aromatics present in the oil. This conclusion is consistent with previous research, which discussed that the aromatics present in the oil are the major precursors for gums and resins formed during heating. They are also the major compounds that cause fouling upon heating. (48)



**Figure 21: Percentage aromatics by weight vs. solids prevented using THFA**

From the above results, two major observations can be made. The first observation is that the amount of solids prevented by adding THFA is correlated with the percentage of aromatics by weight in the original oil sample. It is plausible that the effect of THFA is proportional to the number of aromatics in oils, suggesting that THFA acts primarily on the aromatic component. The second observation is that samples that were heated with THFA seem to have a lighter color residue on the filter paper regardless of the amount of solids present. For Example, Sample SLCO-43-SZ, which was heated with THFA, has 0.0613 g of solids, and yet the color is much lighter than sample COND-54-NZ, which was heated without THFA, which has 0.0342 g of solid. The control experiment with LCO36MZ with no heat also shows that THFA changed the color of the filter paper but not the weight of the residue collected. The color observation suggests that THFA doesn't just prevent solids from forming, but it might also be changing the nature of the solids formed from solids to gums since the color resembled that of a gum and

not of a solid residue. Furthermore, the effect on foulant morphology seems to be heat-independent and can happen at room temperature.

## 4.2 Accelerated fouling of indene with THFA

From the previous data, it was clear that THFA's effect was correlated with the concentration of aromatic molecules. Since crude oil is highly complex, the effect of THFA on model compounds was investigated. Since it was deduced that THFA acts on aromatic molecules, several aromatic model compounds were tested for their fouling behavior with THFA. In the literature, indene was identified as a potential model compound for thermos-oxidative fouling (51). Being an aromatic fouling compound, indene was best chosen to represent the aromatic component of the heavy oil. This system yields gums if heated at 100 °C and atmospheric pressure for 48 hours in kerosene solvent. In this work, a wide range of test conditions using indene and kerosene were evaluated to identify reaction conditions that would yield visual solids. It was found that heating at 150 °C and 750 kPa cold air pressure for 48 hours would yield solids. The samples were further left to age for three months to test for autoxidative stability. This part of the thesis investigates qualitative data, so collecting the solids was not a necessary step. Figure 23 shows an example of the solids formed after heating for two days. Figure 23 shows the indene sample after it was heated at 150 °C and 750 kPa cold air pressure without THFA in kerosene solvent.

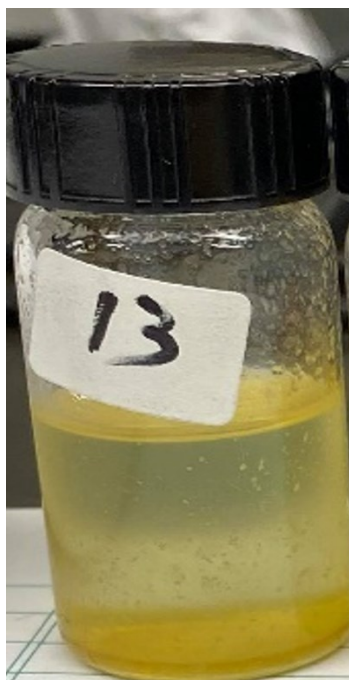


**Figure 22: Visual representation of indene sample after heating at 150 °C and 48 hours with no additives**

The solution shows the appearance of solid particles dispersed across the solution, with no visual signs of any gums formed. The sample was then left to age for three months. Figure 24 shows the aged indene sample after three months of aging.



**Figure 23: Visual representation of aged indene sample after heating at 150 °C with no additives. The sample was aged for three months.**

The sample shows a significant color change to darker yellow, with more solids produced and dispersed all over the solution. Figure 25 shows the indene sample with three wt% THFA after heating for 48 hours.



**Figure 24: Visual representation of indene sample after heating at 150 °C with 3 % THFA. The reaction time was 48 hours.**

The solution shows no visual solids formed or any visual gums sticking to the walls of the vial. A clear solution is observed. Color change to dark orange is also observed. The solution was then left to age for three months. Figure 26 shows the aged indene sample after heating at 150 and 3 wt% THFA.



**Figure 25: Visual representation of aged indene sample after heating at 150 °C with 3 % THFA. Sample aged for three months.**

It can be observed here that the color change across the solution got darker and became less transparent; this is due to dispersed solids forming across the solution. A very thin layer of darker gums settled at the bottom of the vial. This observation implies that there are two different types of solids in the system, one that is dispersed across the solution and heavier gums that settle to the bottom. From this observation, it was suspected that THFA plays a role in the process of solid formation.

To assess the impact of THFA concentration, experiments were conducted with two higher concentrations at 6 and 10 wt% THFA in the indene/kerosene mixture. Results from the experiment with 6 wt% THFA are presented in Figure 27.



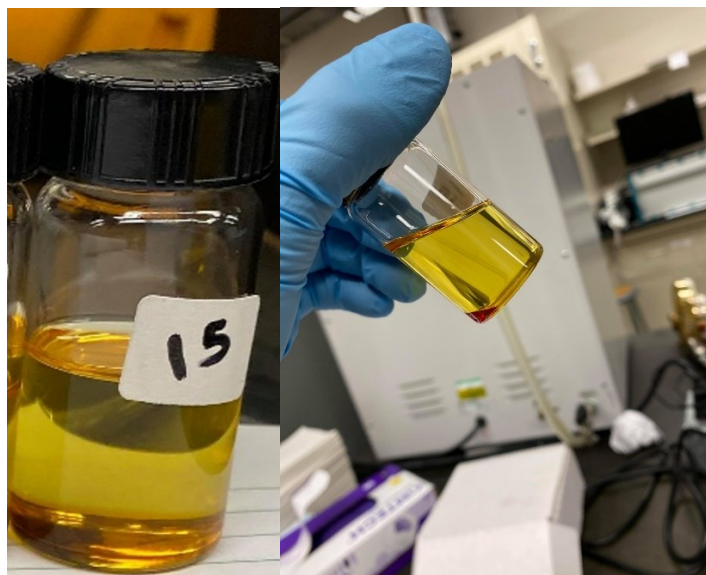
**Figure 26: Visual representation of indene sample after heating at 150 °C with 6 % THFA. The reaction time was 48 hours.**

Figure 27 (sample 12) shows the heated indene solution with 6wt% THFA and 150 °C for 48hrs. The observation on sample 12 initially was that no visible solids were observed visually using the normal eye, but the color change to dark orange was consistent with sample 11. Figure 28 shows the aged indene solution after heating with 6wt% THFA at 150 °C and 48 hours.



**Figure 27: Visual representation of aged indene sample after heating at 150 °C with 6 % THFA**

After three months, it was observed that solid sediments had started forming all across the solution, following the same dispersion trend as sample 11; however, the solution is more transparent. Since the solution is less transparent, it was concluded that fewer solids were dispersed, which implies that higher THFA weight concentration led to fewer solids. It can also be seen that a layer of sticky dark red gum settled at the bottom of the solution. This layer seems more substantial than that of sample 11, which implies that this layer forms due to the presence of the THFA. Figure 29 below shows the heated indene with 10 wt% THFA for 48 hours.



**Figure 28: Visual representation of indene sample after heating at 150 °C with 10% THFA**

Figure 29 (sample 15) shows the heated indene sample with 10wt% THFA yields a similar result to the solutions heated with 3 and 6 wt% THFA, with a more visible red gum settling at the bottom of the vial. The rest of the solution remains clear of any solids. The sample was then left to age for three months. Figure 30 shows the aged sample that was heated with 10 wt% THFA.

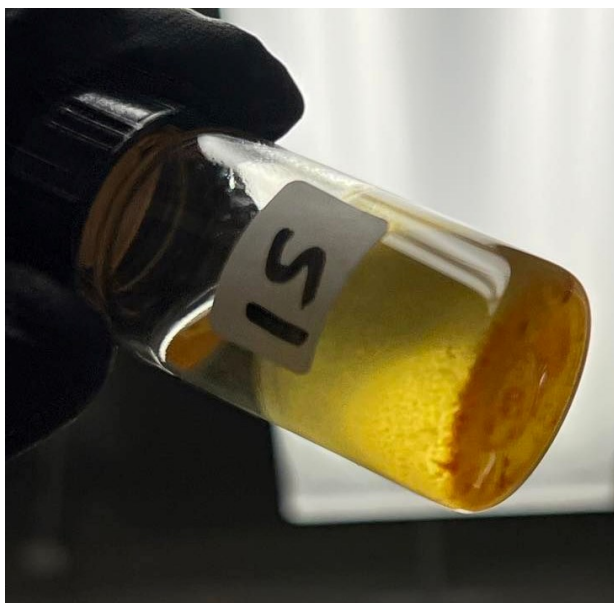


**Figure 29: Visual representation of aged indene sample after heating at 150 °C with 10% THFA**

The solution shows gums forming at the bottom of the vial and also sticking to the vial surface with a smaller amount of dissipated solids closer to the surface of the gums.

When 3% THFA was added, the solution color was darker than those without THFA, some dispersed solids still formed at this lower level of THFA, but a thin layer of liquid dark orange gums formed and settled at the bottom of the vial. These results showed that the presence of THFA contributed to the formation of thick liquid gums.

When 6% THFA was added, fewer solids seemed to form, and more settled gums were formed. This result implies that the presence of THFA doesn't just increase the amount of gums formed but also reduces the formation of dispersed solids overall in the solution.

When 10% THFA was added, more gums formed, and almost no dispersed solids were visually observable. This result was the basis of the assumption that, in the presence of THFA, heating

tends to yield more gums and less dispersed solids. The second step was to determine whether THFA interferes with the chemical reaction physically or chemically or does it just act as a solvent.

Samples 15 and 13 were then dried in the oven at 200 °C until all the upper liquid layers had evaporated. Most of the upper layer of liquid was drained using a pipette, so the samples did not spend significant time inside the oven. Figure 31 shows sample 13 solids after drying in the oven.

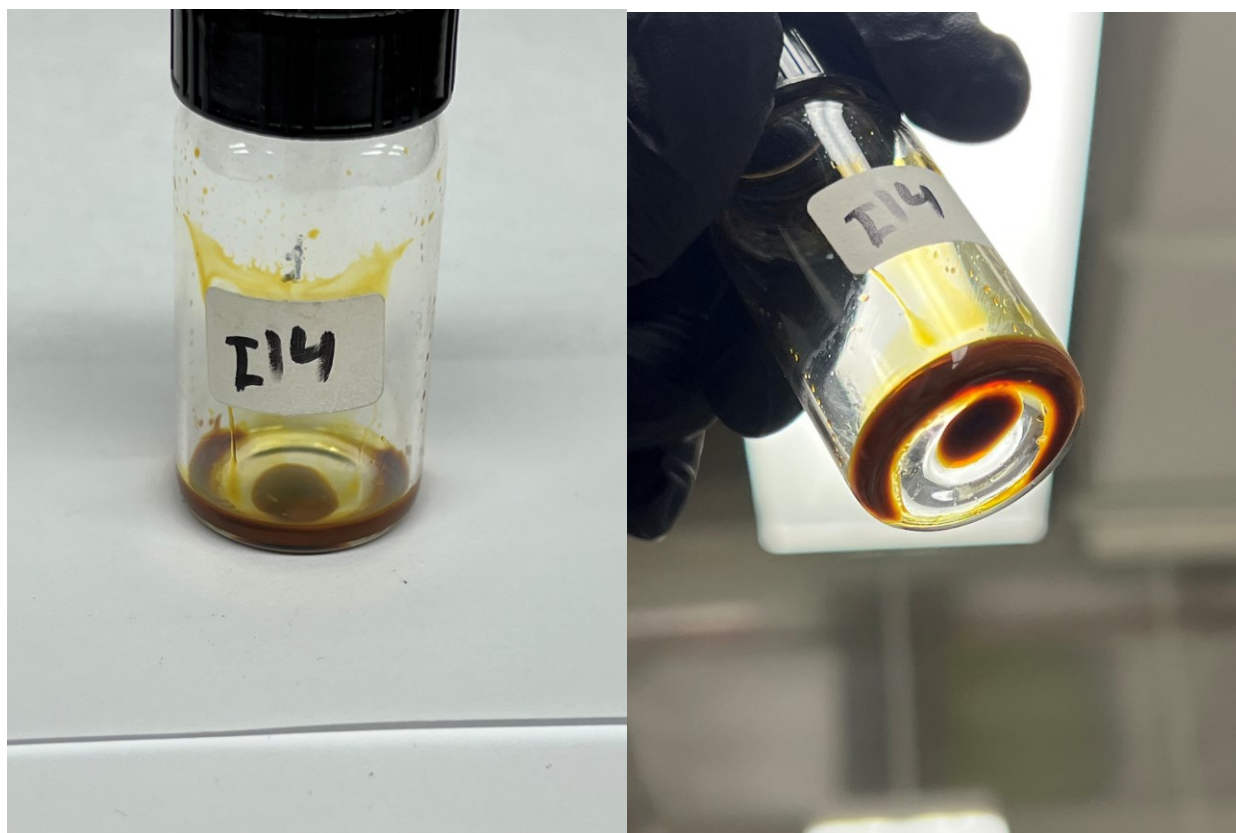


**Figure 30: Visual representation of indene solution after drying in an oven at 200 °C**

On evaporation, the solids have concentrated and formed a darker layer at the bottom of the vial. The solids were very dense but could be scrapped using a metal spatula. Figure 32 shows the dried indene + THFA sample 15.

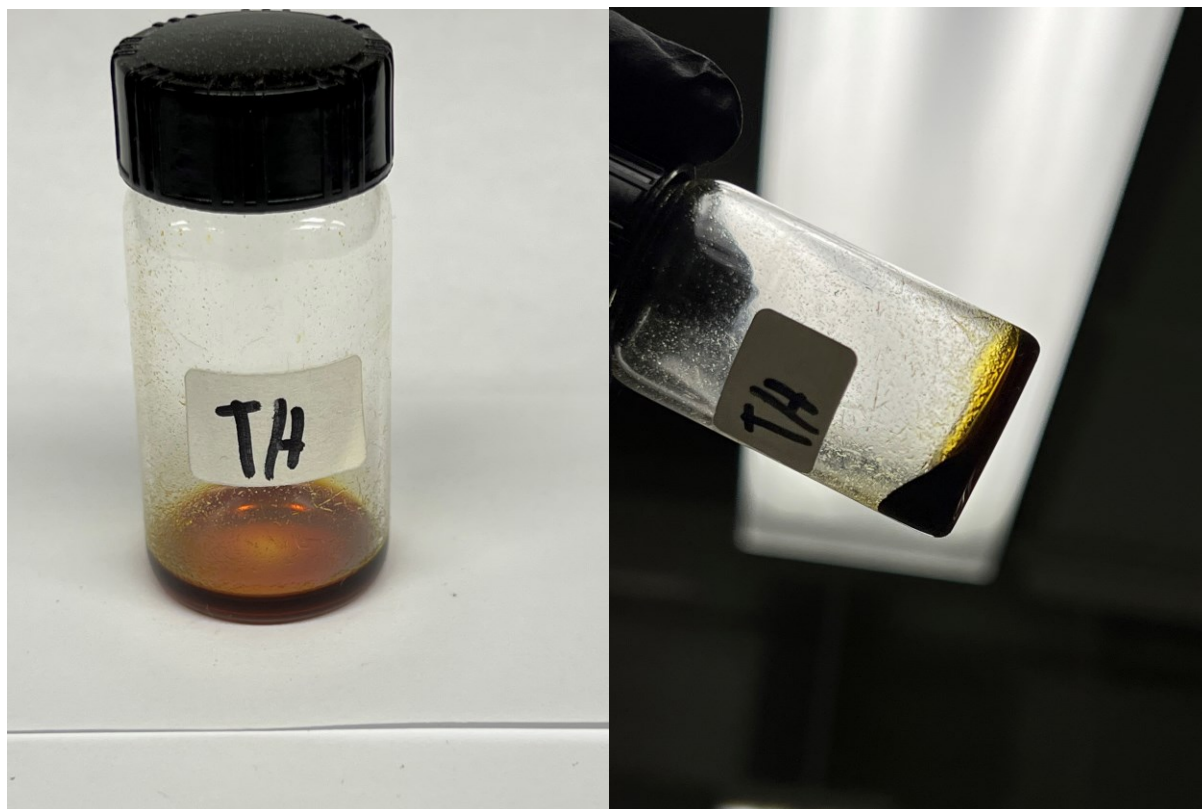


**Figure 31: Visual representation of 1:1 indene with THFA solution after drying in an oven at 200 °C**

The sample contained a heavy thick liquid gum instead of solids which flows very slowly when the vial is tilted. These gums were also very viscous, sticking to the walls and the bottom of the glass vial.

Figure 33 below shows the results from the Thin Layer Paper Chromatography test done on both samples.

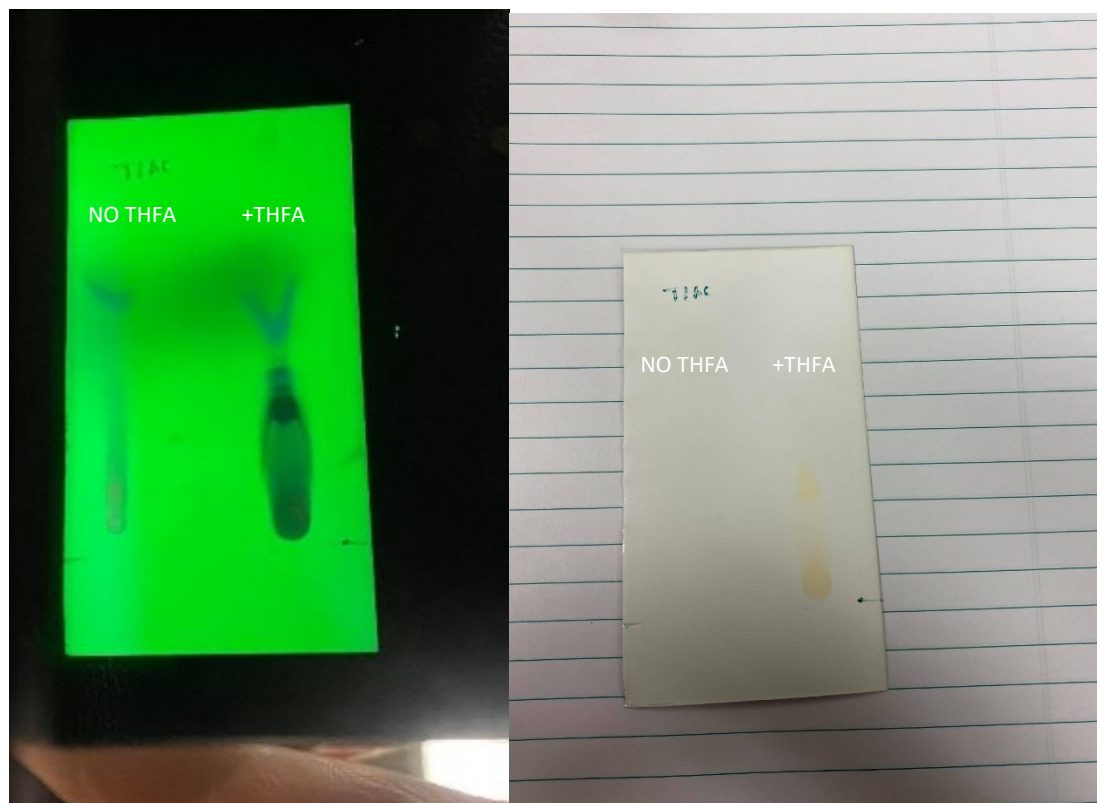


**Figure 32: Visual representation of Chromatography paper results**

The thin layer chromatography for indene showed one peak for indene solids which was not visible until placed in a UV box. For the THFA sample, two spots were found, one which traveled a similar distance as the indene solids while also not being visible until placed under a UV box,

and another one that traveled almost half the distance with a different color, confirming the THFA sample contained two types of products.

Solids and gums are different visually and have different physical behaviors. Solids tend to be finely dispersed for a period of time until enough aggregation happens for them to settle. While gums are much thicker than liquid but freely flow and settle at the bottom of the vial.

The dried samples were also analyzed by FTIR. Figure 34 shows the FTIR spectra carried on sample 13 dried solids

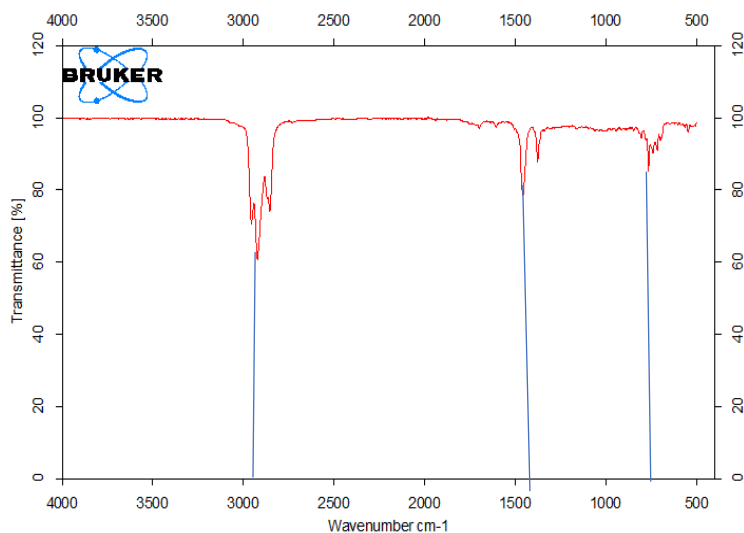


**Figure 33: FTIR spectra of the indene solids**

The FTIR spectroscopy of the dried indene solids showed three peaks at around 3000 cm<sup>-1</sup>, 1400 cm<sup>-1</sup>, and 750 cm<sup>-1</sup>, respectively. It is important to note that the FTIR method used doesn't

detect solids. So, the FTIR detects any liquid trapped inside the solids. Figure 35 shows the FTIR spectra of sample 15 dried indene + THFA gums.

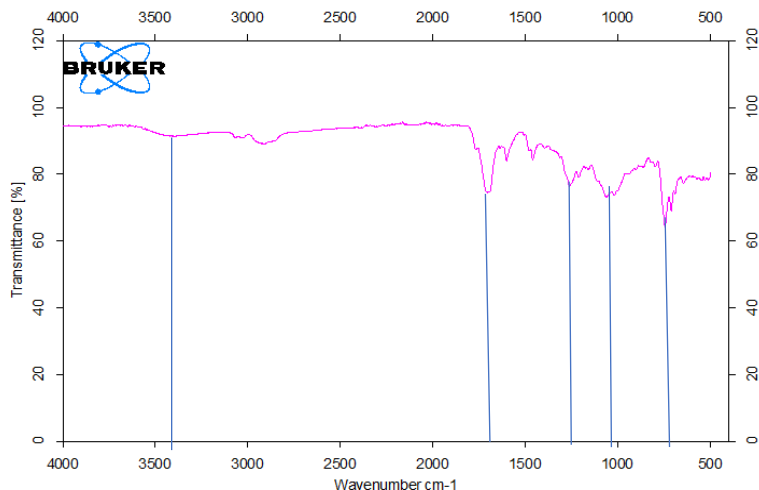


**Figure 34: FTIR spectra of the indene + THFA gums**

The FTIR shows peaks at  $3400\text{ cm}^{-1}$ ,  $1750\text{ cm}^{-1}$ ,  $1250\text{ cm}^{-1}$ ,  $1050\text{ cm}^{-1}$  and  $750\text{ cm}^{-1}$  respectively. The two FTIR spectra show that the chemical structure of the gums and the solids are different, which implies that the presence of THFA contributes chemically to the system. Physically from observing the systems, the gums produced using THFA were different than the solids; the gums acted more like a liquid than a solid. The chromatography test confirmed that the physical structure of the gums was different than the solids. The chromatography test also suggested that the system using THFA exhibited two types of residues. It was shown that out of the different concentrations of the THFA, the most effective was a 1:1 wt.% THFA: aromatic indene molecule. It is important to note that the drying was carried at  $200\text{ }^{\circ}\text{C}$ , which is higher than the boiling temperature of THFA; this means that the dried samples should have minimal residual

THFA, and the effect of THFA producing gums instead of solids remained even after the samples were heated until no more THFA was present.

The FTIR shows clear evidence that the addition of THFA contributed chemically to the system and not just physically. The next step was to determine when the THFA act was and what it does. This was done by analyzing the reaction mixture at different times, before heating, after heating, and after aging. Figure 36 shows the FTIR spectra for the indene solution before heating with three peaks at  $3000\text{ cm}^{-1}$ ,  $1400\text{ cm}^{-1}$ , and  $750\text{ cm}^{-1}$ , respectively. Figure 37 shows the FTIR on the indene mixture after heating for 48 hours.

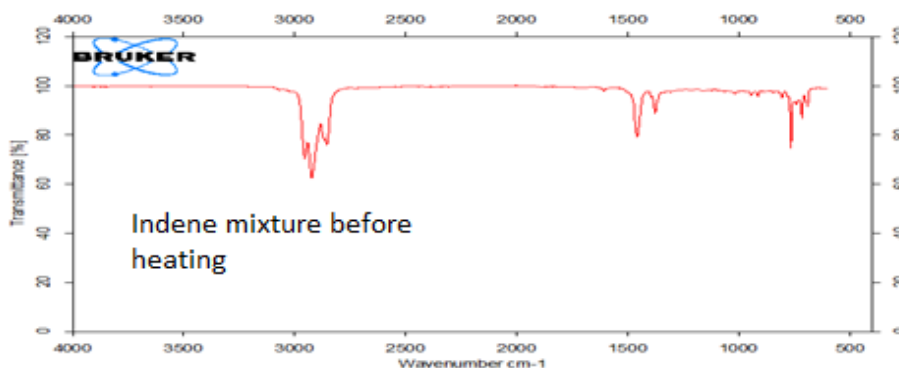


Figure 35: FTIR spectra of indene solution with no additives before heating.

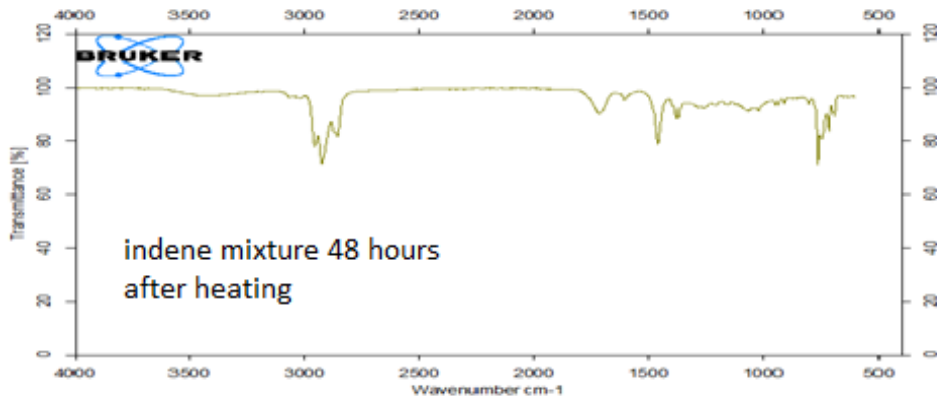
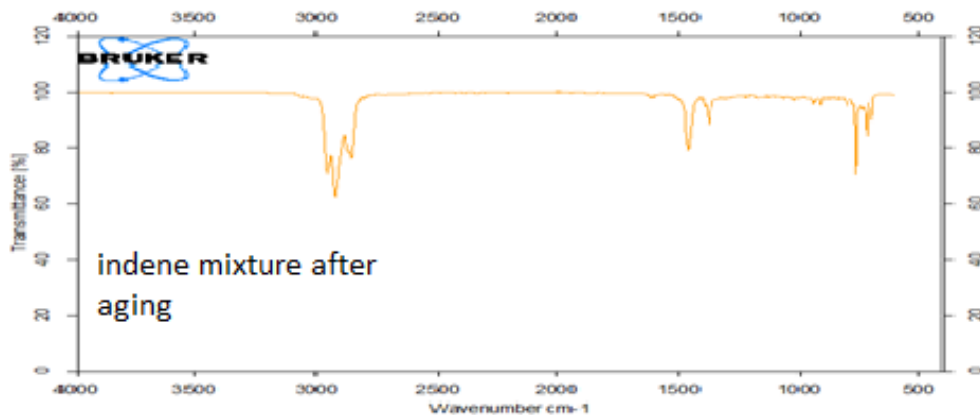


Figure 36: Indene FTIR spectra after heating reaction mixture at  $150\text{ }^{\circ}\text{C}$  for 48 hours.

After 48 hours of mixing, the reaction has not finished as Wilson (54) suggested; the autoxidation of indene in kerosene solvent takes up to 50+ hours, and solids continue to form. Wilson suggested that this effect occurs at 100 °C; however, there was no literature data showing that autoxidation stops at 50 hours at higher temperatures. This result suggests that at this point, the reaction is still taking place, and any new peaks shown in the spectra are either contributed by the products formed or any intermediates forming at this point in the reaction timeline. It is important to note that this spectrum was done at room temperature and not 150 °C, so the reaction was quenched at the 48h point in time. The FTIR used a method that detects only liquid, any functional groups present, is being contributed from the liquid phase. Once solids start forming, the FTIR method is unable to detect them. The insensitivity of FTIR spectroscopy to solids means that if a peak disappears, it could be because the entire molecule containing this functional group solidified or the specific functional group has reacted away.

The FTIR shows two new peaks, a small peak at the hydroxyl group at about 3400  $\text{cm}^{-1}$  and another one at the carbonyl group at about 1750  $\text{cm}^{-1}$ . This observation agrees with the literature (45) where the autoxidation of aromatics produced a hydroxyl group and a carbonyl group. These observations also indicate that the molecules contributing to this peak are still in liquid form. Figure 38 shows the FTIR spectrum of the solution after aging for three months.



**Figure 37: aged Indene solution with no additives**

The spectrum doesn't show any new significant peaks as well; however, it shows the disappearance of the carbonyl peak at  $1750\text{ cm}^{-1}$  and the hydroxyl peak at  $3500\text{ cm}^{-1}$ . This result suggests that the reaction was still taking place at room temperature but much slower. The disappearances of the peaks suggest one of two things, either the bonds have reacted away, or that the molecules have all solidified, forming solids that were not detected by the FTIR analysis. These molecules could also have been just an unstable intermediate. Figure 39 shows a timeline comparison for the FTIR of the three samples before and after heating as well as after aging.

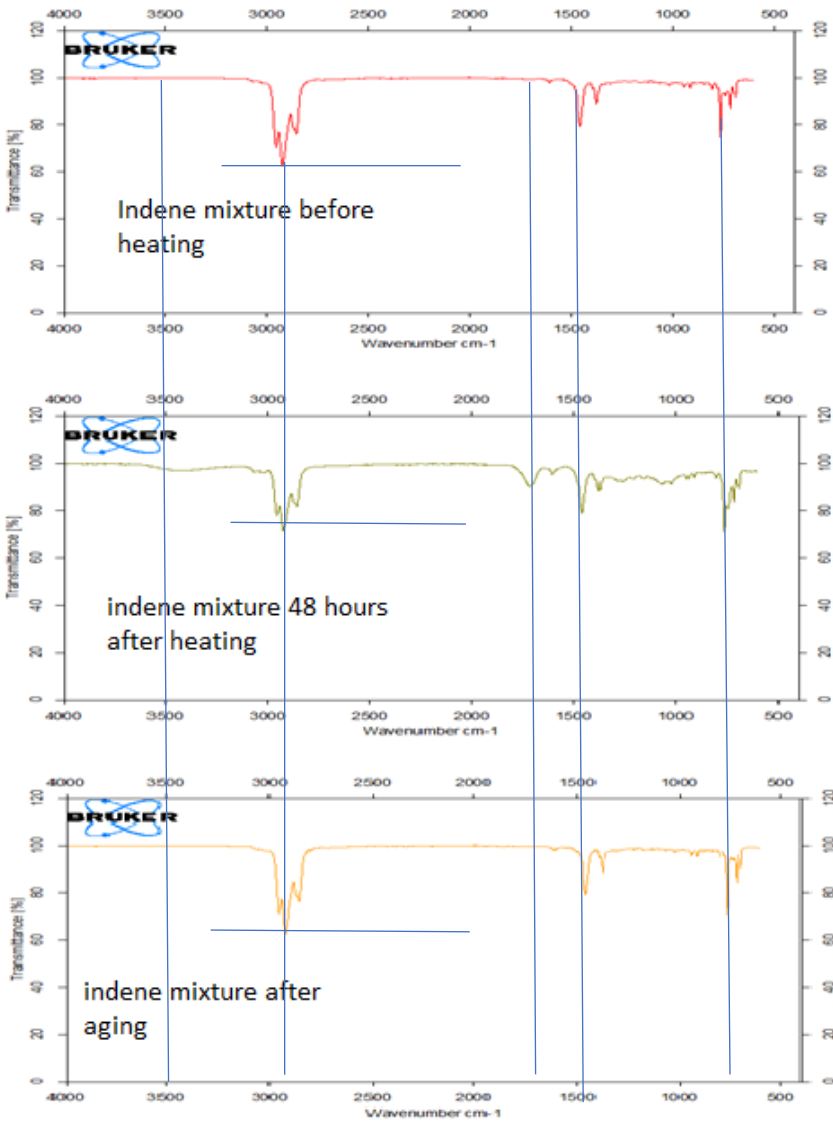


Figure 38: Comparison of the indene solution before heating, after heating, and after aging

Figures 40, 41, and 42 show the FTIR spectra of the indene + THFA mixture before heating, after heating, and after aging, respectively.

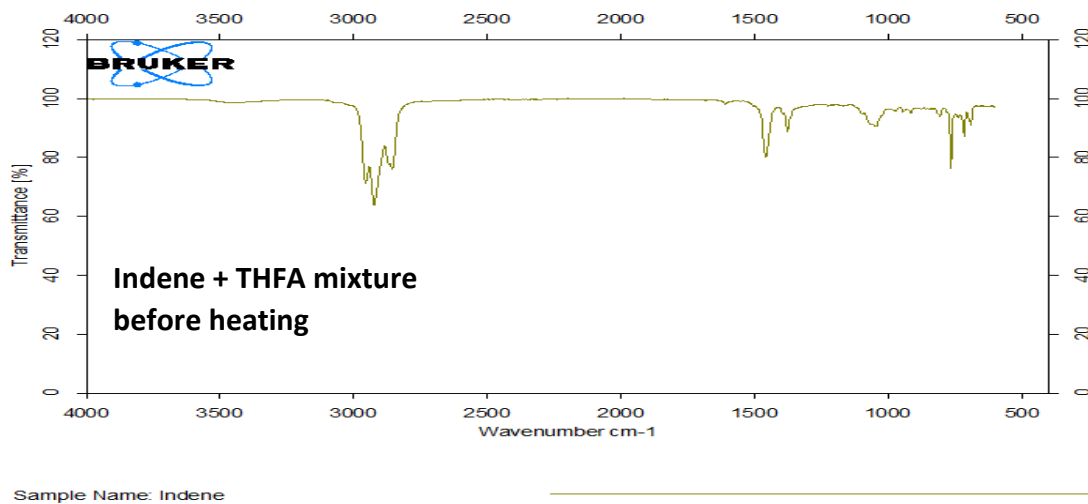


Figure 39: FTIR spectrum of the indene solution with 10% THFA before heating

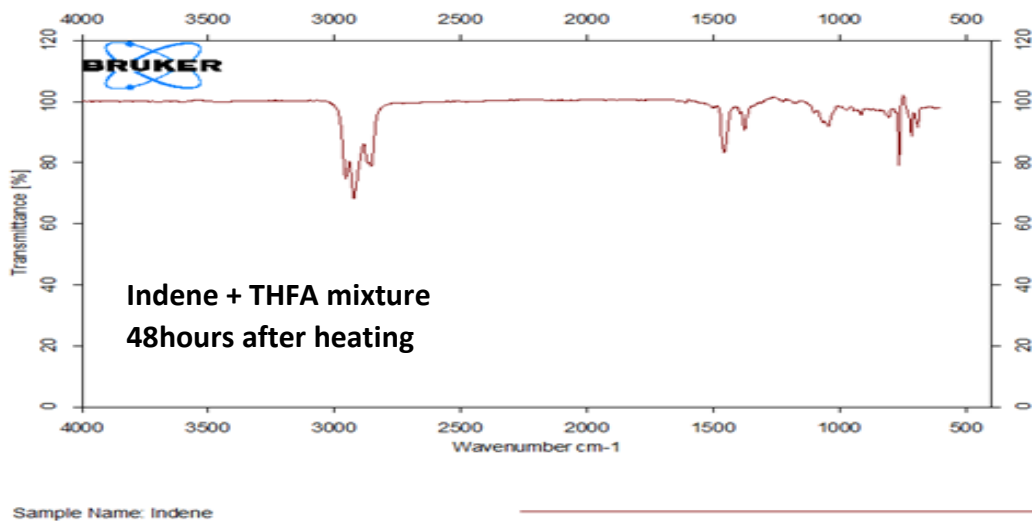
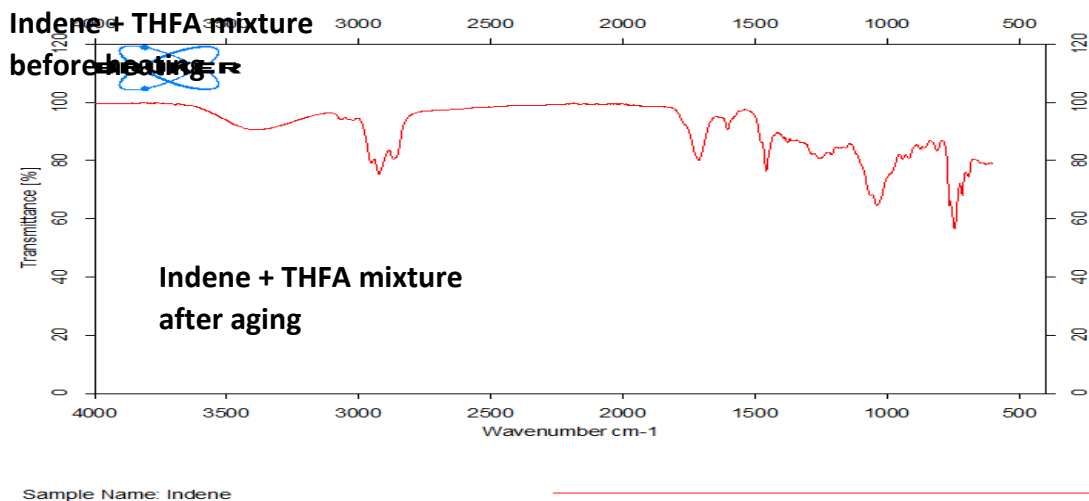


Figure 40: FTIR spectrum of the indene solution with 10% THFA after heating



**Figure 41: FTIR spectrum of the aged indene solution after heating with 10 wt.% THFA**

The FTIR spectra in Figures 40 to 42 show similar peaks to the indene-only solution with two major exceptions, a peak at about  $1050\text{ cm}^{-1}$  is the ether group in the THFA molecule, and the other exception, which is not visible, is the disappearance of the hydroxyl group from the THFA molecule. After heating, no major changes were detected by the FTIR. After aging, a broad OH peak at about  $3500\text{ cm}^{-1}$  has appeared. The shape of the  $3000\text{ cm}^{-1}$  peak has changed as well as its intensity being reduced. A sharp peak at  $1750\text{ cm}^{-1}$  has appeared. A small peak at about  $1250\text{ cm}^{-1}$  has also appeared. The intensity of the  $1050$  peak, which contributes to the ether bond's intensity, has increased as well. Figure 43 below shows a comparison between all 3 FTIR spectra taken.

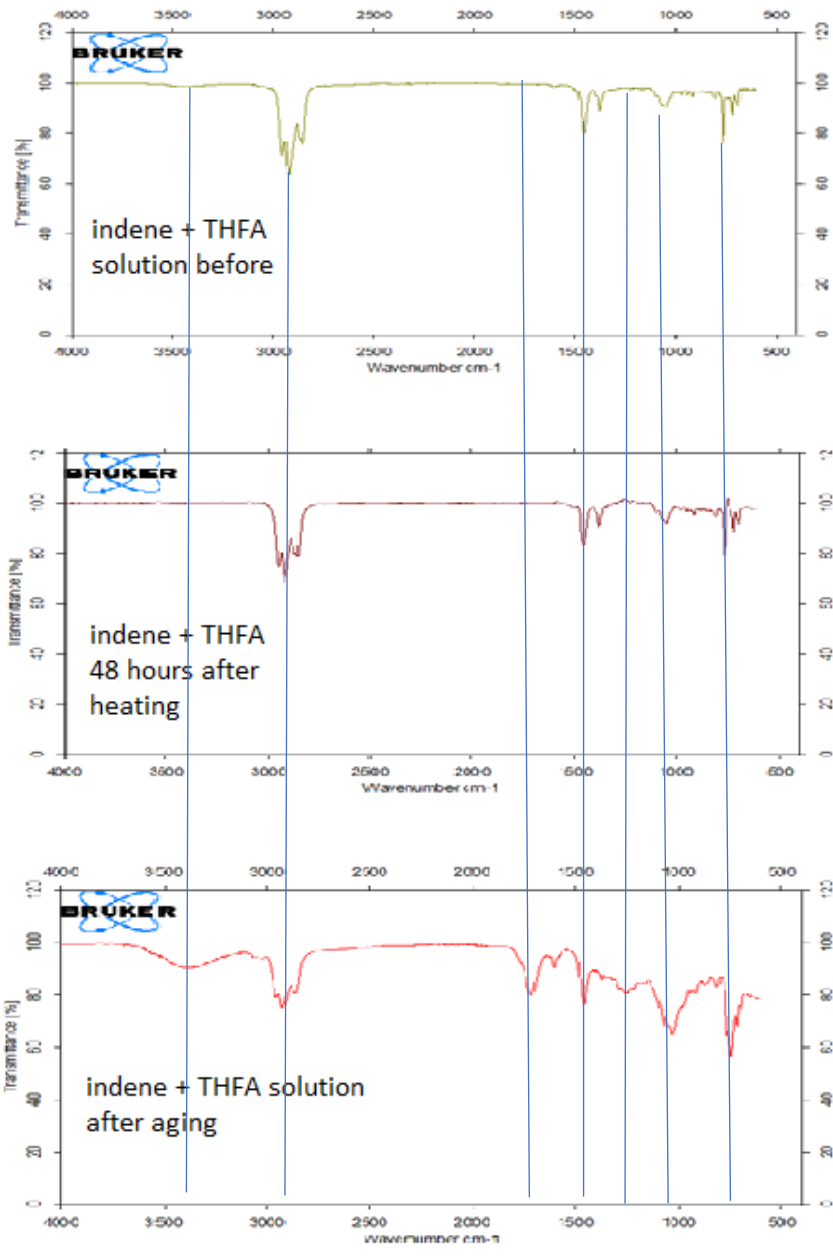
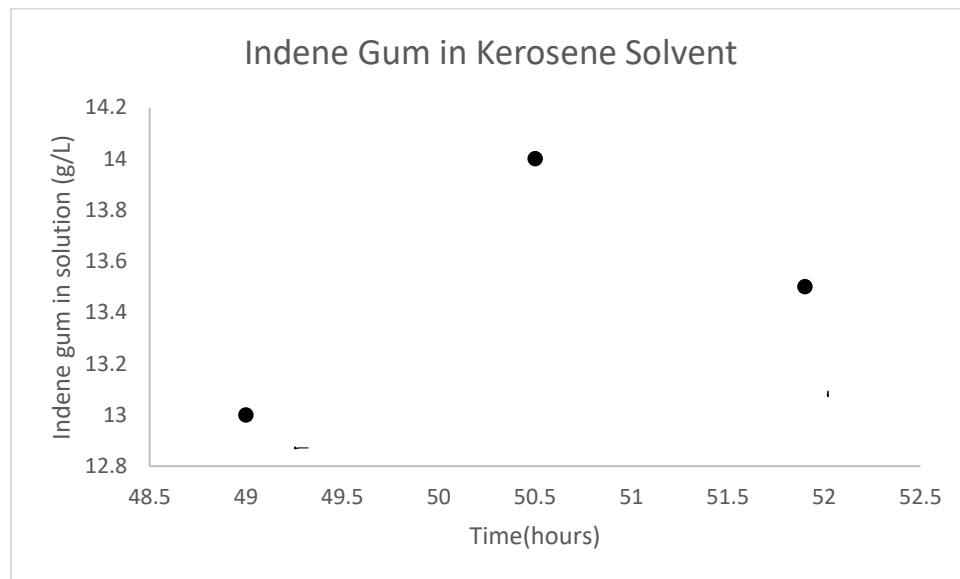


Figure 42: Comparison of the indene solution with THFA before heating, after heating, and after aging

From the above FTIR results, a few observations could be made. The alcohol peak at about 3500  $\text{cm}^{-1}$  shows after aging the solution. It seems that the properties of the mixture have changed, and the OH group is visible again. The OH group has also been reported to be a product of aging and oxidation, so the intensity of this peak is not only contributed by THFA but also by oxidation. (48) The shape of the peak at 3000  $\text{cm}^{-1}$  changes as well, with its intensity decreased. The ether group at 1050  $\text{cm}^{-1}$  is longer and broader.

A peak appearing at 1750  $\text{cm}^{-1}$  is also a product of autoxidation; this peak represents the carbonyl bond forming. (48) Unlike the indene-only mixture, the 1750  $\text{cm}^{-1}$  peak shows and stays stable when THFA is present; it doesn't disappear. This functionality is one of the most important aspects of THFA. The compound which contains the carbonyl group is oxidized further and solidifies without the presence of THFA; however, when THFA is added before heating, this compound forms and stabilizes and doesn't oxidize further. Even when THFA is heated and evaporated and completely leaves the system, its effect on the stability of this compound remains. This observation means that the presence of THFA has changed the chemical structure of this compound to a stable structure which is liquid instead of solid, while still maintaining the carbonyl group.

Figure 44 below shows the product of the auto-oxidation of indene in different solvents. The black dots represent the concentration of indene gums formed during heating vs. time in hours.



**Figure 43: Indene Gum in solution (g/L) vs. time in different solvents during heating. (adapted from (54))**

From Figure 44, the formation of indene gums in solution continued even past the 48 hours point in time. This implies that at 48 hours, the reaction was still taking place and had not finished yet. This conclusion leads to the idea that the FTIR spectra at the 48-hour point in time would show reactants, intermediates, and not just stable products. Since the product solidifies and the FTIR spectra method detects liquids only, the peaks present would be for any remaining reactants that have not reacted yet, and any intermediates present in the solution which are in the liquid phase.

This observation indicates that the carbonyl peak at  $1750\text{ cm}^{-1}$  peak, which showed in the indene-only solution, could potentially be for an intermediate that formed during the reaction

and later disappeared due to solidification or to further reactions. The auto-oxidation fouling model was investigated by Carlson and Robb (35).

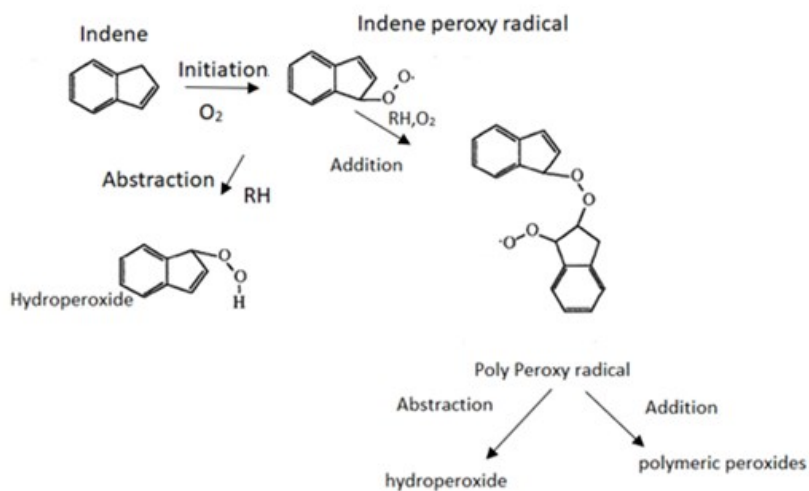


**Figure 44: Autoxidation mechanism for indene(35)**

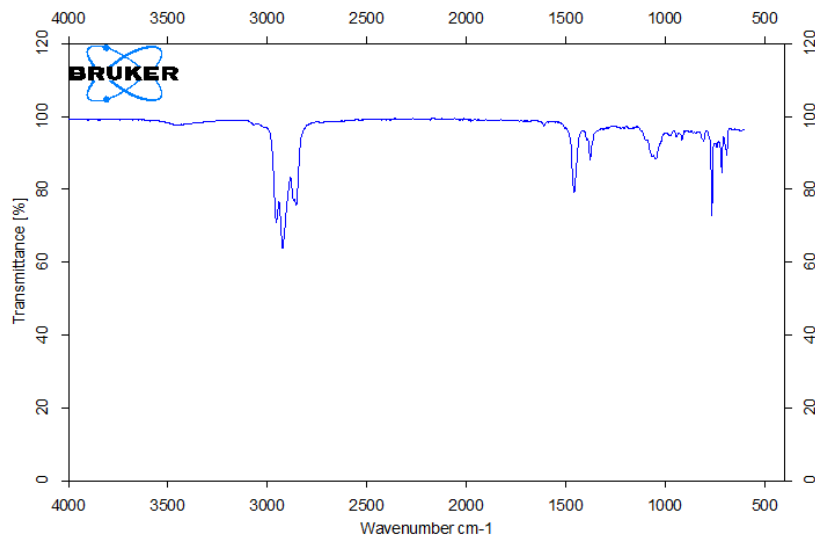
The model shows that the auto-oxidation of indene involves an initiation step that produces free radicals; these radicals could then undergo addition or abstraction to produce solid peroxides. The model was studied at 70 to 95 °C. From the FTIR spectra obtained on the indene solution after heating at 150 °C, the presence of a carbonyl group is not presented in this model. This means that when heated at 150 °C, the autoxidation of indene produced different products.

## 4.3 Accelerated fouling of indene with THFA at higher temperatures

The experiment was repeated at higher temperatures to see the extent of THFA on the thermal stability of the aromatic molecule. The FTIR was taken on the mixture 48 hours after heating and three months after aging.

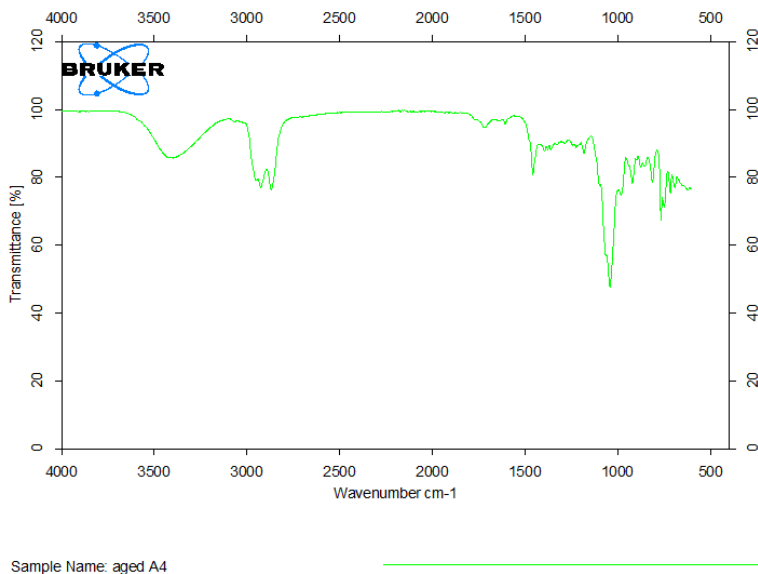
### 4.3.1 Heating indene with THFA at 200 °C

Figure 46 shows the FTIR spectrum of the indene plus THFA after heating at 200 °C for 48 hours, and Figure 47 shows the FTIR spectrum of the sample after aging for three months.



Sample Name: A4

**Figure 45: Indene plus THFA spectra after heating at 200 °C**



**Figure 46: Aged Indene plus THFA spectra after heating at 200 °C**

The FTIR of the solution that was heated at 200 °C right after heating shows a very small peak at the OH group at about 3500  $\text{cm}^{-1}$  and a peak at 3000  $\text{cm}^{-1}$ . The carbonyl region at about 1750  $\text{cm}^{-1}$  shows no visible peaks. The ether bond at 1100  $\text{cm}^{-1}$  is visible.

The FTIR spectra of the aged solution that was heated at 200 °C show a significant peak at the OH region at around 3500  $\text{cm}^{-1}$ . The shape of the peak at about 3000  $\text{cm}^{-1}$  significantly changes as well as its height. A slight peak at the carbonyl region at about 1750  $\text{cm}^{-1}$  cm starts appearing and the ether bond peak intensifies greatly. As for the visual representation, it follows the same trend as heating at 150 °C. the solution turns yellowish with some heavy red thick gum mixture forming at the bottom of the mixture. Figure 48 shows the visual representation of the indene sample with THFA after heating for 48 hours at 200 °C.

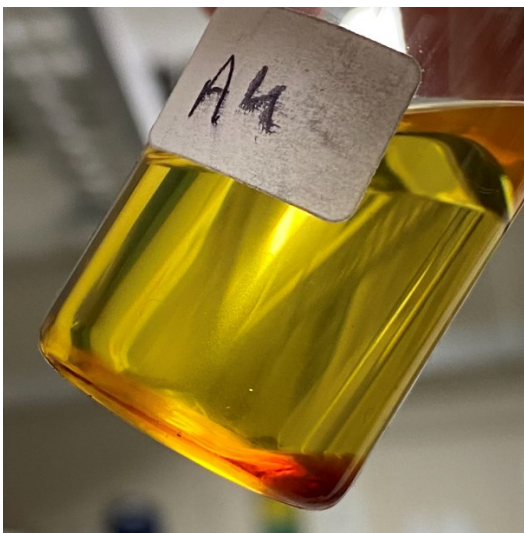


**Figure 47: Indene plus THFA spectra after heating at 200 °C**

It can be observed that the solution is clear of any solids. Two layers of liquid seem to be observed. A heavy reddish layer settled at the bottom of the vial. Figure 49 shows the visual representation of the indene plus THFA that were heated at 200 °C after aging.

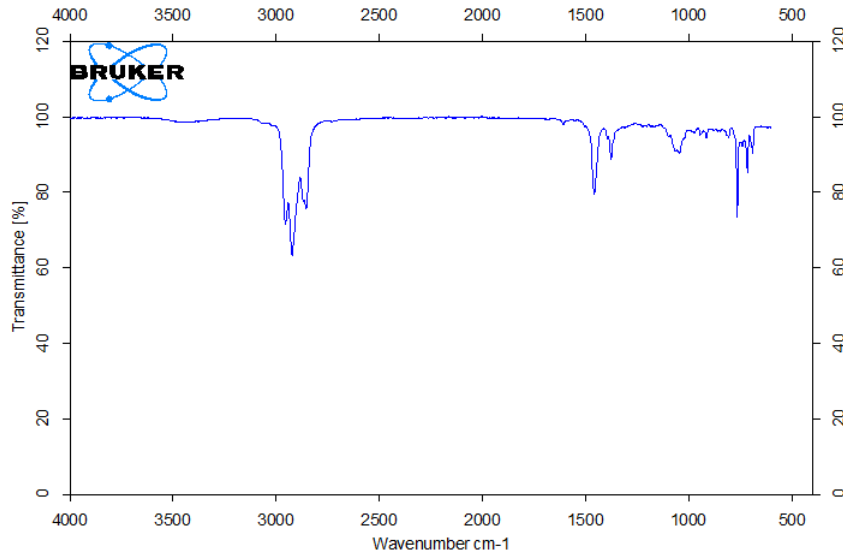


**Figure 48 Visual representation of the aged Indene +THFA mixture after heating at 200 °C.**

The heavy reddish layer that settled at the bottom of the vial has turned into thick gums resembling the previous gums formed at lower temperatures. No solids are observed in the mixture.

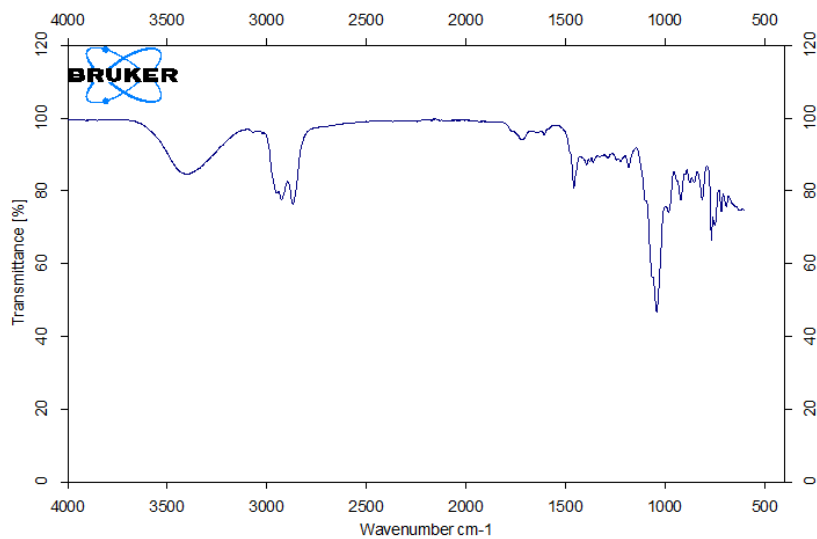
### 4.3.2 Heating Indene with THFA at 230 °C

Figures 50 and 51 show the FTIR spectra of the indene plus THFA after heating and after aging, respectively.



Sample Name: A71

**Figure 49: Indene +THFA spectra after heating at 230 °C**



Sample Name: aged A71

**Figure 50: Aged Indene plus THFA spectra after heating at 230 °C**

Figures 52 and 53 show the visual representation of the indene plus THFA mixture after heating and after aging, respectively.

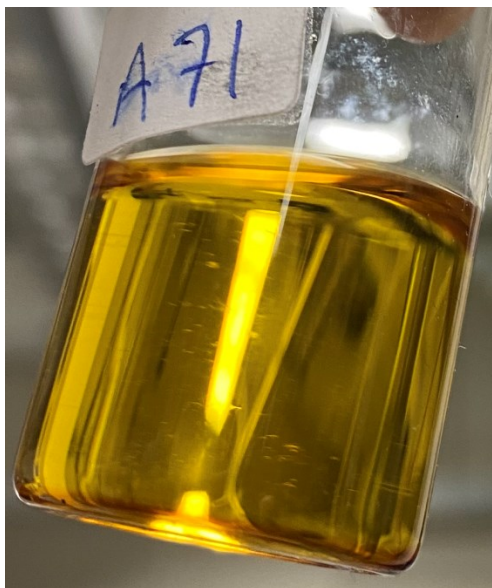


**Figure 51: Visual representation of Indene plus THFA mixture after heating at 230 °C**

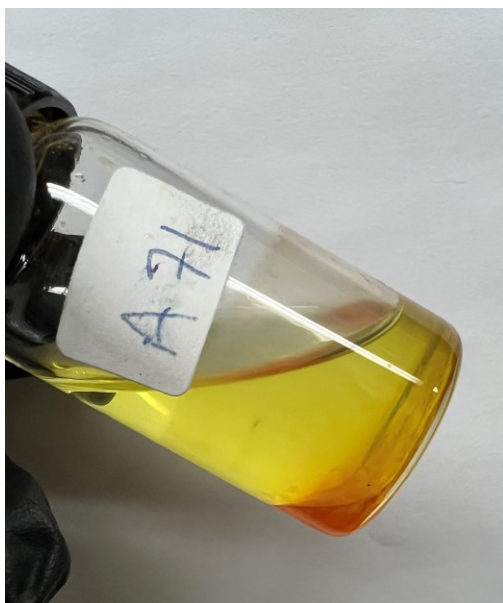


**Figure 52: Visual representation of the aged Indene +THFA mixture after heating at 230 °C**

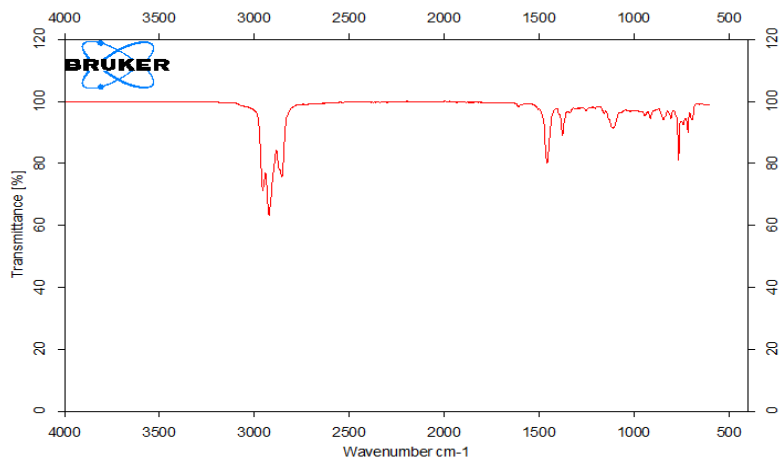
The FTIR of the solution, as well as the visual results, follow the same exact trend at heating at 200 °C and 230 °C. The FTIR spectra show a slight peak at the alcohol region right after heating. No peaks were observed at the carbonyl region, while the ether bond peak was observed at about 1050  $\text{cm}^{-1}$ . After aging, the OH peak intensifies, the aromatics C-H peak at 3000  $\text{cm}^{-1}$  changes shape, and the carbonyl peak at about 1750  $\text{cm}^{-1}$  starts appearing. At the same time, the ether bond peak starts intensifying. Physically, the solution shows a small layer of gums formed right after heating, with no solids. After aging, the layer of gums intensifies, with some solids forming only inside the layer of gums or around it.

## 4.4 Accelerated fouling of indene with ether at higher temperatures

In the preceding sections, while the addition of THFA affected the course of the reaction, the reaction chemistry of THFA addition couldn't be linked to an exact functional group. THFA has both a hydroxyl and an ether functional group. To isolate the effect of the functional groups, a cyclic ether was chosen to replicate the experiment.

### 4.4.1 Heating indene with ether at 150 °C

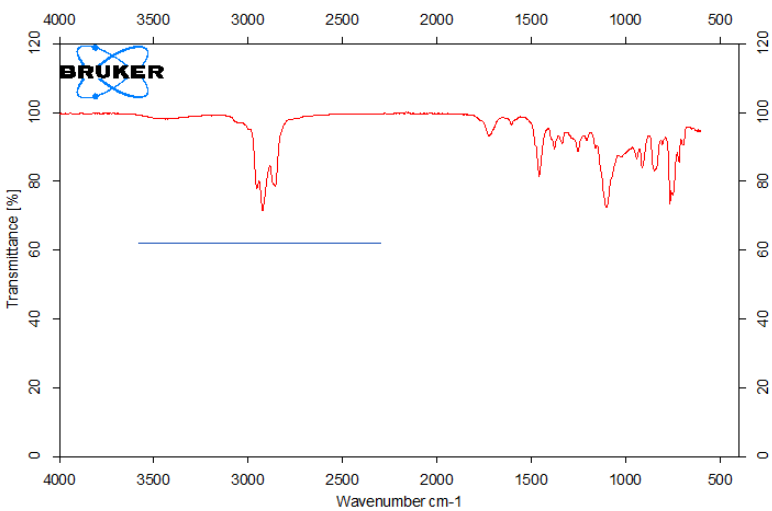
Figures 54 and 55 show the FTIR spectra of the indene plus ether mixture after heating and after aging.



Sample Name: a1

---

**Figure 53: Indene + ether FTIR spectrum after heating at 150 °C for 48 hours**



Sample Name: aged A1

---

**Figure 54: Aged indene + ether FTIR spectrum after heating at 150 °C for 48 hours**

Figures 56 and 57 show the visual representation of the indene + ether mixture after heating and after aging.

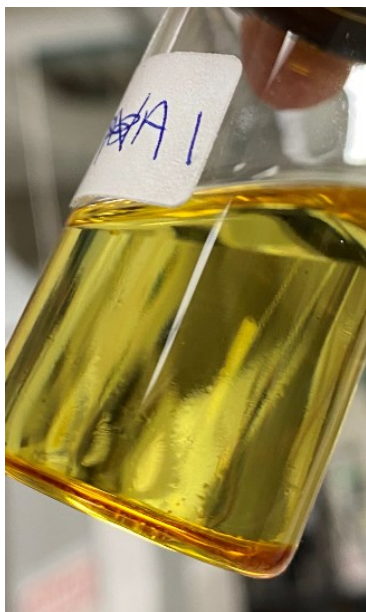


**Figure 55: Visual representation of indene + ether mixture after heating at 150 °C and 48 hours**

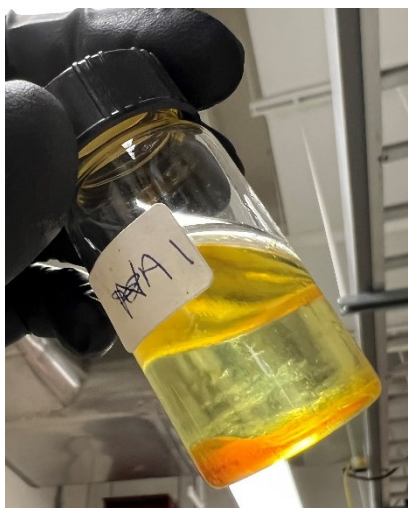
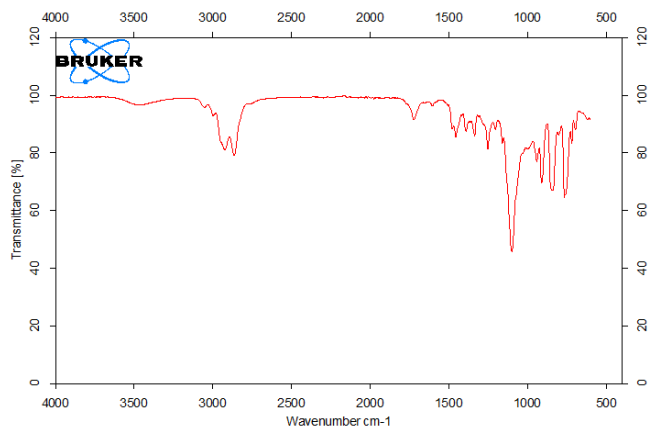


**Figure 56: Visual representation of the aged indene + ether after heating at 150 °C and 48 hours**

The FTIR spectra of the reaction products from heated indene plus ether at 150 °C showed no significant peaks at the OH region and no significant peaks at the carbonyl region after heating. However, after aging, the FTIR spectra show a slight peak at the alcohol region, a decrease in intensity and change of shape at the aromatics C-H peaks at 3000  $\text{cm}^{-1}$ , and the appearance of a peak at the 1750  $\text{cm}^{-1}$  region. The ether peak at about 1100  $\text{cm}^{-1}$  also intensifies. The visual observations of the two samples with ether follow a similar trend to the indene samples heated with THFA. At first, after heating, a small layer of heavy liquid gum is present at the bottom of the glass vial, with the rest of the solution remaining clear of any solids with a yellow–brown color. After further aging, the sample shows a significant increase in the heavy liquid gum layer, and the nature of the gum changes, becoming stickier as shown in the picture; some of the gums remain sticking to the bottom of the glass vial.

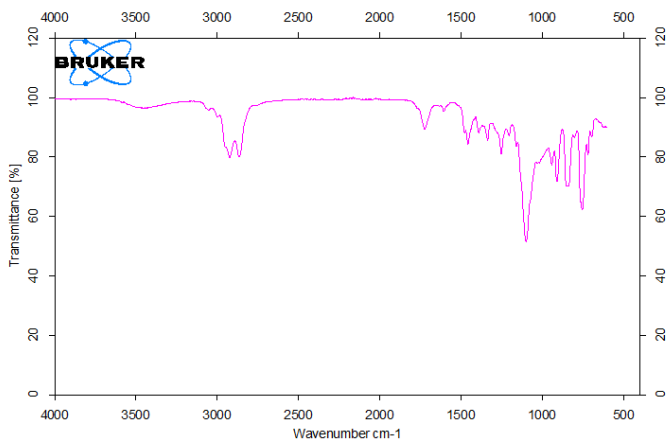
#### 4.4.2 Heating indene with ether at 200 °C

Figures 58 and 59 show the FTIR spectra of the indene plus ether mixture after heating and after aging.



Sample Name: A5

**Figure 57: Indene + ether FTIR spectrum after heating at 200 °C and 48 hours**



Sample Name: aged A5

**Figure 58: Aged indene + ether FTIR spectrum after heating at 200 °C and 48 hours**

Figures 60 and 51 show the visual representation of the indene plus ether mixture after heating and after aging.

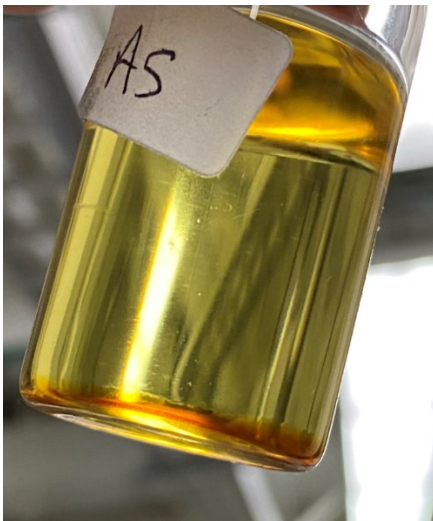


**Figure 59: Visual representation of the indene + ether mixture after heating at 200 °C and 48 hours**

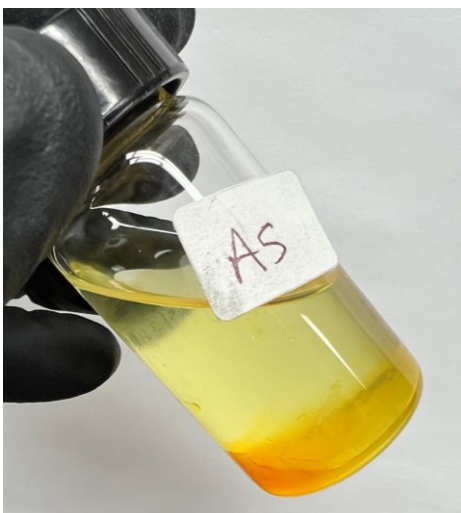
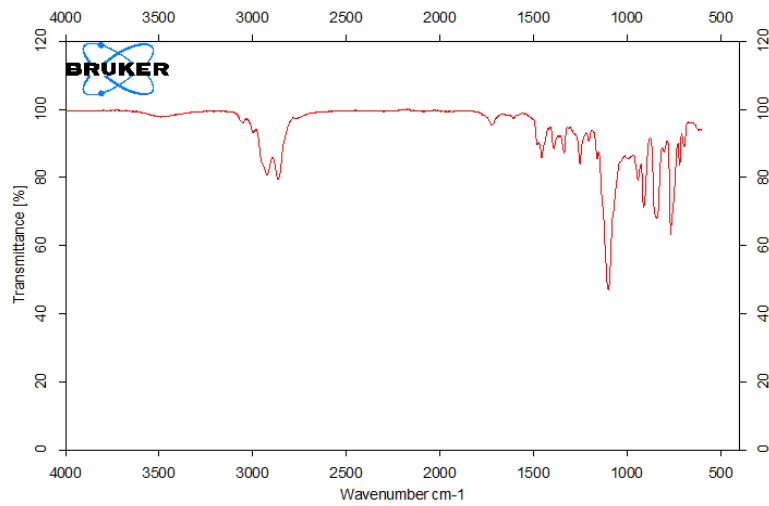


**Figure 60: Visual representation of the aged indene + ether mixture after heating at 200 °C and 48 hours**

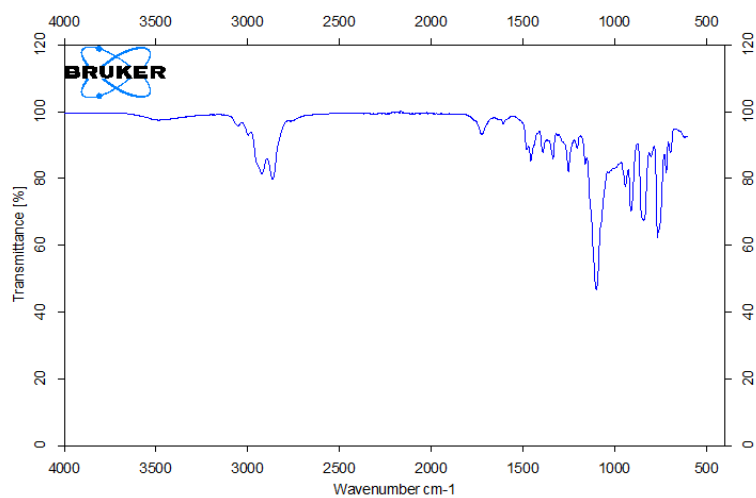
### 4.4.3 Heating indene with ether at 230 °C

Figures 62 and 63 show the FTIR spectra of the indene plus ether mixture after heating and after aging.



Sample Name: A81

**Figure 61: Indene plus ether FTIR spectrum after heating at 230 °C and 48 hours**



Sample Name: aged A81

**Figure 62: Aged indene plus ether FTIR spectrum after heating at 230 °C and 48 hours**

Figures 64 and 65 show the visual representation of the indene + ether mixture after heating and after aging.



**Figure 63: Visual representation of the indene + ether mixture after heating at 230 °C and 48 hours**

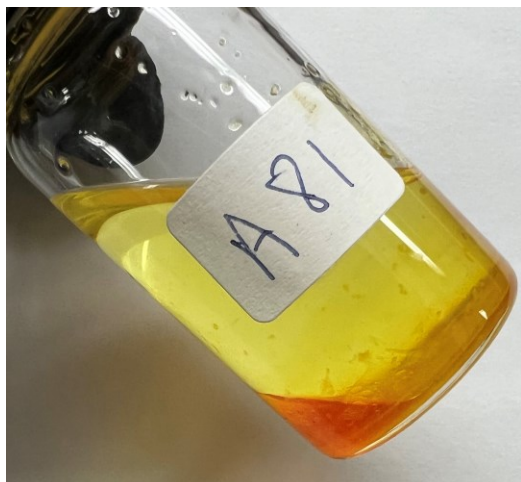


**Figure 64: Visual representation of the aged indene + ether mixture after heating at 230 °C and 48 hours**

The analysis of reaction products from heated indene plus ether generated at 200 and 230 °C show that the ether failed at preventing the formation of the hydroxyl and the carbonyl groups after heating for 48 hours.

The above observations show a trend and a link between the physical appearance and the chemical analysis done. For this discussion, the results from the oil samples will be described separately from the indene samples.

- A.** First, for the samples of oils that were heated, it was noticed that THFA had two effects on the samples.
- 1) Gravimetric analysis showed that the addition of THFA reduced the amount of filterable material from reaction products.

- 2) Colorimetric analysis of the residual filterable solids demonstrated that when THFA was added to the reaction mixture, the products were much lighter in color than when THFA was not added. This observation was independent of the mass of products generated from a reaction. This observation suggested that the presence of THFA doesn't only prevent solids from forming but also changes their nature to gums; since gums are filterable, they could be weighted but show a lighter color on the filter paper.
- 3) In the control samples, when THFA was added to the oil without heat, there was no change in the weight of the filterable solids; however, the color of the filter paper faded. This observation suggests that THFA's effect in changing the nature of solids to gums is temperature independent.

Figure 66 shows a summary of the thermal oxidation of Heavy oil with and without THFA.

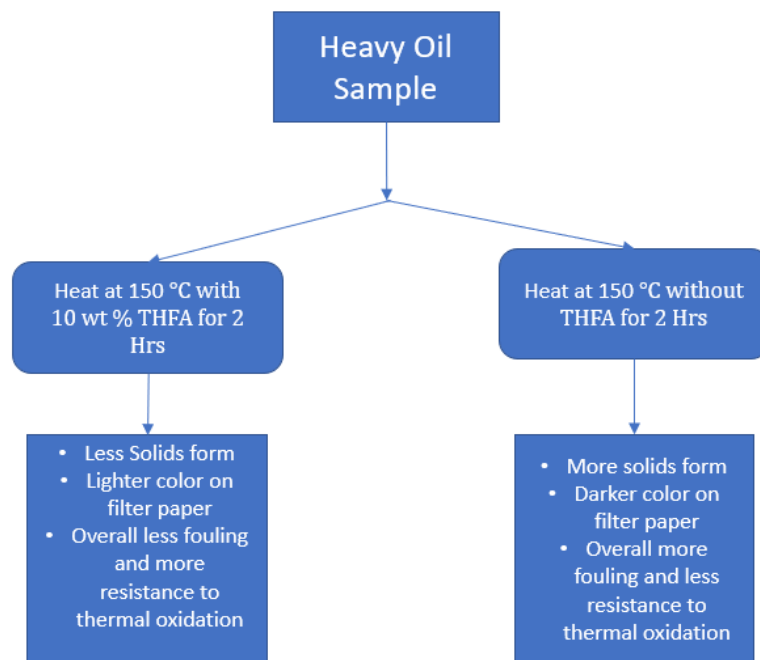


**Figure 65: Summary of Heavy oil thermal oxidation with THFA**

**B.** For the indene samples that were heated with different concentrations of THFA, the following observations were made.

- 1) The samples showed both solids and gums forming when THFA concentration was less than 1:1 with respect to indene.
- 2) Most gums formed, and the least solids formed when a ratio of 1:1 THFA to indene was present. This suggests that THFA acts directly on the aromatic indene molecule.
- 3) The solids formed were dispersed all over the solution while the gums heavily settled at the bottom of the solution.

C. For the indene samples that were heated with THFA at a ratio of 1:1 at 150, 200, and 230 °C, respectively.

- 1) The FTIR spectra that were taken after the 48 h heating process showed no carbonyl group or OH group.
- 2) No solids were found in the solution but a layer of gum.
- 3) When the samples were aged, peaks at the OH region started appearing, a decrease in intensity and change of shape at the 3000  $\text{cm}^{-1}$  peak, a slight peak at the carbonyl region at about 1750  $\text{cm}^{-1}$ , and the ether bond at about 1100  $\text{cm}^{-1}$  intensified.
- 4) The physical representation showed that gums start forming only after aging and after the chemical observations in 3) were observed.

These observations suggest that the presence of THFA delays the oxidation to a carbonyl group and delays the oxidation to a hydroxyl group. Changes the nature of the solids formed from solids to gums, the fact that the OH group intensifies, and the ether group intensifies as well, the OH peak intensifies in most samples. However, with THFA the OH group intensifies significantly more, and that is because the OH bond which is contributed by the THFA molecule is visible again. This result suggests the recyclability of the THFA molecules; this observation also supports the patents released in the use of THFA. (28,29)

Analysis of the experimental data shows that THFA has two effects on this system:

- i. Delaying the thermal autoxidation.
- ii. Changing the physical nature of the products of the autoxidation from solids to heavier gums.

**D. For the indene samples heated with ether**

- 1) The addition of ether to the reaction mixture showed similar effects to THFA at 150 °C, delaying the autoxidation and changing the nature of solids to gums.
- 2) The specific ether used in the experiments failed to prevent thermal autoxidation at the higher temperatures of 200 and 230 °C; the results after heating were the same as the results that were observed after the aging of the other runs.

Figure 67 shows a summary of the products formed from the thermal oxidation of indene with and without additives at different temperatures.

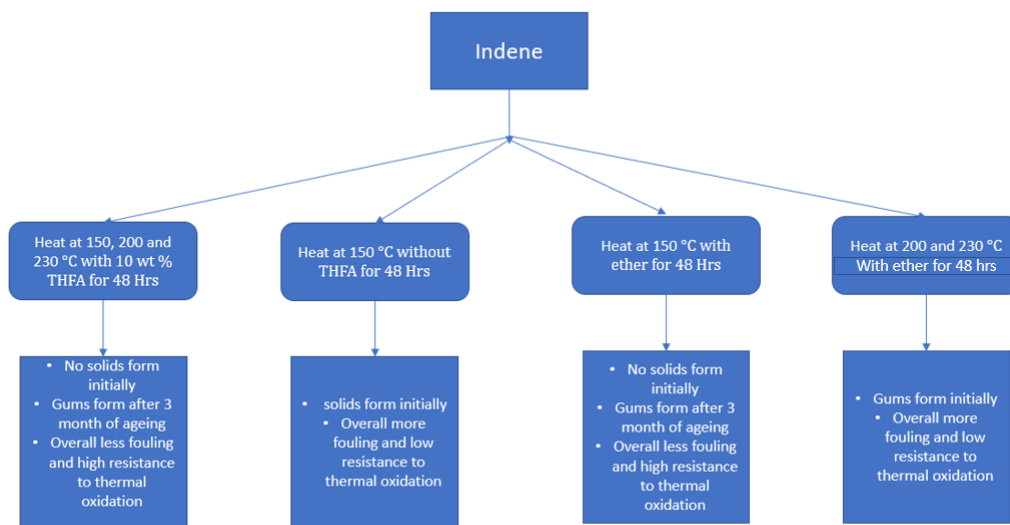


**Figure 66: Summary of Indene thermal oxidation with THFA and Ether Additives**

## 5 Conclusion

From the above observations, few conclusions could be drawn; the thermal autoxidation of the indene at 150 °C degrees follows two steps; the first step involves the production of hydroxyl groups and carbonyl groups, while these groups stay in the liquid phase for some time if the samples are aged long enough, these groups eventually undergo a second step which involves the formation of solids, the nature of the second step has not been thoroughly investigated in this thesis, whether the molecules further oxidize or do they simply aggregate to form solids is not yet known. The presence of THFA during heating does two things to the system; it slows down the first step, which produces the carbonyl and hydroxyl group, and the second thing THFA does is that it leads to the formation of liquid gums instead of solids. The exact mechanism of how THFA does this effect is also unknown since the mechanism of the step itself is unknown. If the molecules aggregate, then THFA could be stopping their aggregation or changing the path at which they aggregate, leading to gums, and if the molecules do oxidize or react further, THFA could be inhibiting the reaction, leading to a different chemical reaction which also forms gums.

From the drying test, THFA shows that its effect is permanent on the system; even after the molecule was completely evaporated in the oven at 200 °C, which is higher than the boiling point of THFA (178 °C), the remaining product was a dark liquid sticky gum, vs. dark solids produced by the indene.

On the samples of the oil that were heated at 150 °C, gums were also produced in the presence of THFA and not solids. This effect of THFA seems to be effective up to 230 °C of heating. The ether showed a similar effect to THFA at the 150 °C heating; however, it completely failed when the solution was heated at a higher temperature of 200 and 230 °C. This suggests that the ether bond in THFA is involved in the mechanism, as well as the OH bond.

## REFERENCES

- (1) The Shell Bitumen Industrial Handbook. (1995).
- (2) (2020, November 11). Bitumen upgrading explained. Oil Sands Magazine. Retrieved October 26, 2022, from <https://www.oilsandsmagazine.com/technical/bitumen-upgrading>
- (3) Rice, F. O., & Herzfeld, K. F. (1934). The thermal decomposition of organic compounds from the standpoint of free radicals. vi. the mechanism of some chain reactions. *Journal of the American Chemical Society*, 56(2), 284–289. <https://doi.org/10.1021/ja01317a006>
- (4) Kossiakoff, A., & Rice, F. O. (1943). Thermal decomposition of hydrocarbons, resonance stabilization and isomerization of free radicals1. *Journal of the American Chemical Society*, 65(4), 590–595. <https://doi.org/10.1021/ja01244a028>
- (5) Gray, M. R., & McCaffrey, W. C. (2002). Role of chain reactions and olefin formation in cracking, hydroconversion, and coking of petroleum and bitumen fractions. *Energy & Fuels*, 16(3), 756–766. <https://doi.org/10.1021/ef010243s>
- (6) Savage, P. E., & Klein, M. T. (1987). Asphaltene Reaction Pathways. 2. pyrolysis of N-pentadecylbenzene. *Industrial & Engineering Chemistry Research*, 26(3), 488–494. <https://doi.org/10.1021/ie00063a015>
- (7) Savage, P. E., & Klein, M. T. (1988). Asphaltene Reaction Pathways. 4. pyrolysis of tridecylcyclohexane and 2-ethyltetralin. *Industrial & Engineering Chemistry Research*, 27(8), 1348–1356. <https://doi.org/10.1021/ie00080a003>
- (8) DENTE, M. E., & RANZI, E. M. (1984). Cheminform abstract: Mathematical modeling of hydrocarbon pyrolysis reactions. *Chemischer Informationsdienst*, 15(7). <https://doi.org/10.1002/chin.198407335>

- (9) Hauser, A., Stanislaus, A., Marafi, A., & Al-Adwani, A. (2005). Initial coke deposition on hydrotreating catalysts. part II. structure elucidation of initial coke on hydrodematallation catalysts. *Fuel*, 84(2-3), 259–269. <https://doi.org/10.1016/j.fuel.2004.08.010>
- (10) Xiong, Z., Syed-Hassan, S. S., Xu, J., Wang, Y., Hu, S., Su, S., Zhang, S., & Xiang, J. (2018). Evolution of coke structures during the pyrolysis of bio-oil at various temperatures and heating rates. *Journal of Analytical and Applied Pyrolysis*, 134, 336–342. <https://doi.org/10.1016/j.jaap.2018.06.023>
- (11) He, W., Liu, Z., Liu, Q., Ci, D., Lievens, C., & Guo, X. (2014). Behaviors of radical fragments in tar generated from pyrolysis of 4 Coals. *Fuel*, 134, 375–380. <https://doi.org/10.1016/j.fuel.2014.05.064>
- (12) Meng, X., Xu, C., & Gao, J. (2007). Coking behavior and catalyst deactivation for catalytic pyrolysis of heavy oil. *Fuel*, 86(12-13), 1720–1726. <https://doi.org/10.1016/j.fuel.2006.12.023>
- (13) Wiehe, I. A. (1993). A phase-separation kinetic model for Coke Formation. *Industrial & Engineering Chemistry Research*, 32(11), 2447–2454. <https://doi.org/10.1021/ie00023a001>
- (14) Shamsi, A., Baltrus, J. P., & Spivey, J. J. (2005). Characterization of coke deposited on PT/alumina catalyst during reforming of liquid hydrocarbons. *Applied Catalysis A: General*, 293, 145–152. <https://doi.org/10.1016/j.apcata.2005.07.002>
- (15) Yan, Y., Shi, L., Liu, Q., Shi, X., Wang, T., Zhou, Q., Liu, Z., Han, W., & Li, M. (2017). Coke and radicals formation on a sulfided nimo/ $\gamma$ -al<sub>2</sub>O<sub>3</sub> catalyst during hydroprocessing of an atmospheric residue in hydrogen donor media. *Fuel Processing Technology*, 159, 404–411. <https://doi.org/10.1016/j.fuproc.2017.02.005>
- (16) Callejas, M. A., Martínez M.T., Blasco, T., & Sastre, E. (2001). Coke characterisation in aged residue hydrotreating catalysts by solid-state <sup>13</sup>C-NMR spectroscopy and temperature-

programmed oxidation. *Applied Catalysis A: General*, 218(1-2), 181–188.

[https://doi.org/10.1016/s0926-860x\(01\)00640-8](https://doi.org/10.1016/s0926-860x(01)00640-8)

- (17) Akmaz, S., Gurkaynak, M. A., & Yasar, M. (2012). The effect of temperature on the molecular structure of Raman asphaltenes during pyrolysis. *Journal of Analytical and Applied Pyrolysis*, 96, 139–145. <https://doi.org/10.1016/j.jaap.2012.03.015>
- (18) Gonçalves, M. L., Ribeiro, D. A., Teixeira, A. M., & Teixeira, M. A. (2007). Influence of asphaltenes on Coke Formation during the thermal cracking of different Brazilian distillation residues. *Fuel*, 86(4), 619–623. <https://doi.org/10.1016/j.fuel.2006.08.022>
- (19) McCaffrey, W. C.; Cameron, R. A.; Gray, M. R. Physical behavior of bitumen under rapid heating. *ACS Div. Pet. Chem. Rep.* 1998, 43 (4), 616.
- (20) Gray, M. R., Le, T., McCaffrey, W. C., Berruti, F., Soundararajan, S., Chan, E., Huq, I., & Thorne, C. (2001). Coupling of mass transfer and reaction in coking of thin films of an Athabasca vacuum residue. *Industrial & Engineering Chemistry Research*, 40(15), 3317–3324. <https://doi.org/10.1021/ie0009379>
- (21) Vafi, K. (2012). High temperature thermal cracking of heavy oils. PhD thesis, University of Alberta, Edmonton.
- (22) Yang, Z., Li, G., Yuan, H., Liu, G., & Zhang, X. (2017). Efficient coke inhibition in supercritical thermal cracking of hydrocarbon fuels by a little ethanol over a bifunctional coating. *Energy & Fuels*, 31(7), 7060–7068. <https://doi.org/10.1021/acs.energyfuels.7b01505>
- (23) Merat, N., Godawa, C., & Gaset, A. (2007). High selective production of tetrahydrofurfuryl alcohol: Catalytic hydrogenation of furfural and furfuryl alcohol. *Journal of Chemical Technology & Biotechnology*, 48(2), 145–159. <https://doi.org/10.1002/jctb.280480205>
- (24) Chen, X., Sun, W., Xiao, N., Yan, Y., & Liu, S. (2007). Experimental study for liquid phase selective hydrogenation of furfuryl alcohol to tetrahydrofurfuryl alcohol on supported Ni

- catalysts. *Chemical Engineering Journal*, 126(1), 5–11.  
<https://doi.org/10.1016/j.cej.2006.08.019>
- (25) Matsagar, B. M., Hsu, C.-Y., Chen, S. S., Ahamad, T., Alshehri, S. M., Tsang, D. C., & Wu, K. C.-W. (2020). Selective hydrogenation of Furfural to tetrahydrofurfuryl alcohol over a reloaded carbon catalyst in aqueous solution under mild conditions. *Sustainable Energy & Fuels*, 4(1), 293–301. <https://doi.org/10.1039/c9se00681h>
- (26) Sunyol, C., English Owen, R., González, M. D., Salagre, P., & Cesteros, Y. (2021). Catalytic hydrogenation of Furfural to tetrahydrofurfuryl alcohol using competitive nickel catalysts supported on mesoporous clays. *Applied Catalysis A: General*, 611, 117903.  
<https://doi.org/10.1016/j.apcata.2020.117903>
- (27) Wang, C., Lee, J. D., Ji, Y., Onn, T. M., Luo, J., Murray, C. B., & Gorte, R. J. (2018). A study of tetrahydrofurfuryl alcohol to 1,5-pentanediol over PT–WOX/c. *Catalysis Letters*, 148(4), 1047–1054. <https://doi.org/10.1007/s10562-018-2323-6>
- (28) Fletcher, L. C., Beard, H. J., & O'Blasny, R. (1982, November 23). Distillation and solvent extraction process for rerefining used lubricating oil (United States, Patent No. US4342645), U.S. Department of Energy, <https://www.osti.gov/biblio/6674831>.
- (29) Oehr, K. H. (2016, January 14). Method of upgrading heavy crude oil ( Canada, Surrey, Patent No. WO2014124517A1) , U.S. Patent and Trademark Office,  
<https://patents.google.com/patent/WO2014124517A1/en>.
- (30) Russell, G. A. (1956). Oxidation of unsaturated Compounds. III. products of the reaction of indene and oxygen; stereochemistry of the addition of a peroxy radical and oxygen to a double bond<sup>1</sup>. *Journal of the American Chemical Society*, 78(5), 1035–1040.  
<https://doi.org/10.1021/ja01586a044>
- (31) Russell, -G. A. (1956). Oxidation of unsaturated Compounds. iv. kinetics of the reaction of indene with oxygen; evidence of the identity of active intermediates in thermal and

- catalyzed oxidations. *Journal of the American Chemical Society*, 78(5), 1041–1044.  
<https://doi.org/10.1021/ja01586a045>
- (32) Ueno, Y., Kotetsu, N. & Yoshida, T. (1974). *Aromatikkusu*, 26, P117-120.
- (33) Morris, R. E., Hazlett, R. N., & McIlvaine, C. L. (1988). The effects of stabilizer additives on the thermal stability of Jet Fuel. *Industrial & Engineering Chemistry Research*, 27(8), 1524–1528. <https://doi.org/10.1021/ie00080a029>
- (34) Morris, R. E., & Mushrush, G. W. (1991). Fuel instability model studies: The liquid-phase cooxidation of thiols and indene by oxygen. *Energy & Fuels*, 5(5), 744–748.  
<https://doi.org/10.1021/ef00029a021>
- (35) Carlsson, D. J., & Robb, J. C. (1966). Liquid-phase oxidation of hydrocarbons. part 4. — indene and tetralin: Occurrence and mechanism of the thermal initiation reaction with oxygen. *Trans. Faraday Soc.*, 62, 3403–3415. <https://doi.org/10.1039/tf9666203403>
- (36) Howard, J. A., & Ingold, K. U. (1963). The inhibited autoxidation of styrene: Part III. the relative inhibiting efficiencies of ortho-alkyl phenols. *Canadian Journal of Chemistry*, 41(11), 2800–2806. <https://doi.org/10.1139/v63-411>
- (37) Stephenson, W.K. & Rowe, C.T. (1993). Fouling control in ethylene recovery systems. *A.I.Ch.E. Symp. Ser.* 295, 89, p335-340.
- (38) SCOTT, G. E. R. A. L. D. (1993). Antioxidants: Chain breaking mechanisms. *Atmospheric Oxidation and Antioxidants*, 121–160. <https://doi.org/10.1016/b978-0-444-89615-5.50008-1>
- (39) Réblová, Z. (2012). Effect of temperature on the antioxidant activity of phenolic acids. *Czech Journal of Food Sciences*, 30(No. 2), 171–175. <https://doi.org/10.17221/57/2011-cjfs>

- (40) ASTM Standard D2274, 2014, Test method for oxidation stability of distillate fuel oil (accelerated method), ASTM International, United States. (n.d.).  
<https://doi.org/10.1520/d2274-03>
- (41) Berthomieu, C., & Hienerwadel, R. (2009). Fourier transform infrared (FTIR) spectroscopy. *Photosynthesis Research*, 101(2-3), 157–170. <https://doi.org/10.1007/s11120-009-9439-x>
- (42) COLTHUP, N. O. R. M. A. N. B., DALY, L. A. W. R. E. N. C. E. H., & WIBERLEY, S. T. E. P. H. E. N. E. (1975). Preface. *Introduction to Infrared and Raman Spectroscopy*, xi-xii.  
<https://doi.org/10.1016/b978-0-12-182552-2.50003-6>
- (43) Knözinger, E. (1986). P. R. Griffiths, J. A. de Haseth: *Fourier Transform Infrared Spectroscopy*, vol. 83 aus der Reihe: *Chemical analysis-a series of monographs of Analytical Chemistry and its applications*, John Wiley + sons, Chichester, New York, Brisbane, Toronto, Singapore. *Berichte Der Bunsengesellschaft Für Physikalische Chemie*, 90(12), 1240–1241. <https://doi.org/10.1002/bbpc.19860901224>
- (44) Deng, H., & Callender, R. (1999). [8] raman spectroscopic studies of the structures, energetics and bond distortions of substrates bound to enzymes. *Methods in Enzymology*, 176–201. [https://doi.org/10.1016/s0076-6879\(99\)08010-6](https://doi.org/10.1016/s0076-6879(99)08010-6)
- (45) Barth, A. (2007). Infrared spectroscopy of proteins. *Biochimica Et Biophysica Acta (BBA) - Bioenergetics*, 1767(9), 1073–1101. <https://doi.org/10.1016/j.bbabi.2007.06.004>
- (46) IR Spectrum Table & Chart. IR Spectrum Table. (n.d.). Retrieved January 9, 2023, from <https://www.sigmaaldrich.com/CA/en/technical-documents/technical-article/analytical-chemistry/photometry-and-reflectometry/ir-spectrum-table>
- (47) Mecozzi, M., Pietroletti, M., Scarpiniti, M., Acquistucci, R., & Conti, M. E. (2011). Monitoring of marine mucilage formation in Italian seas investigated by infrared spectroscopy and independent component analysis. *Environmental Monitoring and Assessment*, 184(10), 6025–6036. <https://doi.org/10.1007/s10661-011-2400-4>

- (48) Czarnocka, J., Matuszewska, A., & Odziemkowska, M. (2015). Autoxidation of fuels during storage. *Storage Stability of Fuels*. <https://doi.org/10.5772/59807>
- (49) Batts, B. D., & Fathoni, A. Z. (1991). A literature review on fuel stability studies with particular emphasis on diesel oil. *Energy & Fuels*, 5(1), 2–21.  
<https://doi.org/10.1021/ef00025a001>
- (50) Pedersen, C. J. (1956). Mechanism of antioxidant action in gasoline. *Industrial & Engineering Chemistry*, 48(10), 1881–1884. <https://doi.org/10.1021/ie50562a036>
- (51) Totten, G., Westbrook, S., & Shah, R. (2003). *Fuels and lubricants handbook: Technology, properties, performance, and testing*. <https://doi.org/10.1520/mnl37-eb>
- (52) Mortier, M., Fox, F., & Orszulik, T. (Eds.). (2010). *Chemistry and Technology of Lubricants*. <https://doi.org/10.1007/978-1-4020-8662-5>
- (53) Rudnick, L. R. (2017). *Additives for Industrial Lubricant Applications*. *Lubricant Additives*, 473–484. <https://doi.org/10.1201/9781315120621-26>
- (54) Wilson, D. I. (1994). *Model experiments of autoxidation reaction fouling*, PhD thesis, The university of British Columbia, Kelowna.
- (55) Palys, D. (2019). *Ex-situ Observation and Characterization of Mild Hydrotreated Liquid Products*, MSc thesis, University of Alberta, Edmonton.